NONLINEAR OPTIMAL CONTROL OF WING ROCK PROBLEM

A Thesis Submitted

n Partial Fulfillment of the Requirements

for the Degree of

Master of Technology

by

AJAY KUMAR SINGH

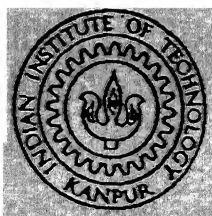

to the

DEPARTMENT OF AEROSPACE ENGINEERING

INDIAN INSTITUTE OF TECHNOLOGY KANPUR

December 1998

NONLINEAR OPTIMAL CONTROL OF WING ROCK PROBLEM

A Thesis Submitted

in Partial Fulfillment of the Requirements

for the Degree of

Master of Technology

by

AJAY KUMAR SINGH

to the

DEPARTMENT OF AEROSPACE ENGINEERING

INDIAN INSTITUTE OF TECHNOLOGY KANPUR

December 1998

CERTIFICATE

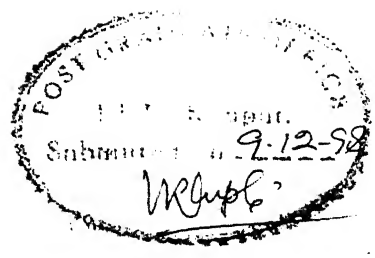

It is certified that the work contained in the thesis entitled **Nonlinear Optimal Control of Wing Rock Problem**, by **Ajay Kumar Singh**, has been carried out under my supervision and that this work has not been submitted elsewhere for a degree.

Dr. Ashish Tewari

Assistant Professor

Department of Aerospace Engineering

Indian Institute of Technology

Kanpur

December, 1998

ACKNOWLEDGEMENT

I wish to express deep sense of gratitude to Dr. Ashish Tewari for giving me the opportunity to work under his able guidance, for his keen interest and constant encouragement.

I shall be failing in my duties if I do not express sincere gratefulness and thanks to my colleagues, Vipin, Shailendra, Raju, Praveen and Prashant for their invaluable help and providing me with a vivacious atmosphere during my stay over here.

Finally, I greatly appreciate the help and inspiration received from my parents and all well wishers.

Date: 21.1.1999 (AJAY KUMAR SINGH)

I.I.T. Kanpur

Abstract

This thesis addresses the optimal control of wing rock problem, which is described by nonlinear equations of motion. A procedure is utilized to obtain optimal control law for a nonlinear system, in which a positive performance index is minimised. The optimality equations are obtained from Hamilton-Jacobi-Bellman equation, which minimises this performance index. The positive definite closed loop Lyapunov function is assumed to have same matrix form as performance index. Earlier, this method had been used for obtaining the solution of second order system, but in this thesis, it had been extended to third and fifth order systems. Both optimal nonlinear and linear feedback cases have been evaluated. It has been observed that both nonlinear as well as linear feedback control are equally efficient in controlling the wing rock motion of the model considered in this thesis at three angles of attack, 21.5 deg, 22.5 deg and 25 deg. A first-order actuator actuator has been incorporated and the effects of sideslip have also been considered. It has been shown that wing rock motion can also be initiated by sideslip even if sideslip angle is very small in magnitude. So, while designing the control system, this factor should also be given equal importance, which has generally been neglected in existing literature. It has also been observed that the simplified assumption made by Monahemi and Krstic that roll angle is twice of sideslip angle may not be applicable.

Contents

List of Figures

NOMENCLATURE

A	=linear system state matrix
a_i	=coefficients dependent on angles of attack
B	=control matrix
b	=wing span (m.)
b_1, b_2	=coefficients of wing rock equation
c	=chord (m.)
C_1, C_2	=constant values
C_l	=aerodynamic roll moment coefficient
C_{lp}	=rolling moment derivative due to roll rate p and sideslip rate $\dot{\beta}$
$C_{l\beta}$	=rolling moment stability derivative due to sideslip angle β
F(x)	=matrix of nonlinear terms
f(x)	=nonlinear terms of the system
H	=Hamiltonian equation
I_x	=roll moment of inertia ($kg - m^2$.)
J	=performance index, also called cost function
k	$=1/\tau$ (s^{-1}.)
L	=rolling moment
L_c	=characteristic length (m.)
L_p	=rolling moment due to roll rate p (s^{-1}.)
L_β	=roll moment due to sideslip angle β (s^{-2}.)
L_r	=roll moment due to yaw rate (s^{-1}.)

n	=positive integer relative to the highest order term of f(x)
N_p	=yaw moment due to roll rate (s^{-1}.)
N_r	=yaw rate damping (s^{-1}.)
N_β	=directional stability (s^{-2}.)
$\mathbf{P}$	=Lyapunov matrix
p	=roll rate (rad/s.)
$\mathbf{P_{i,j}}$	=submatrix of $\mathbf{P}$
$P_{i,j}(i,j)$	=elements of submatrix $\mathbf{P_{i,j}}$
$\mathbf{Q}$	=interpolated terms of q(x)
q	=dynamic pressure (N/m^2.)
$\mathbf{Q_{i,j}}$	=submatrix of $\mathbf{Q}$
$Q_{i,j}(i,j)$	=elements of submatrix $\mathbf{Q_{i,j}}$
q(x)	=nonlinear state performance index
$\mathbf{R}$	=control weight matrix
S	=wing reference area (m^2.)
T	=transpose of a matrix
t	=time (s.)
T^*	=terminal time (s.)
t^*	=nondimensional time
$\mathbf{u}$	=control inputs
U_c	=characteristic speed (m/s.)
V	=freestream air speed (m/s.)
V(x)	=Lyapunov function
w	=wing rock limit cycle frequency (s^{-1}.)
$\mathbf{x}$	=system state variables
α	=angle of attack (deg.)
β	=sideslip angle (rad.)
γ	=yaw angle (deg.)
δ_A	=aileron angle (rad.)
$\delta_{A_{COM}}$	=commanded aileron angle (rad.)

θ	=apex half angle (deg.)
$\bar{\theta}$	=effective apex angle (deg.)
μ_1, μ_2	=coefficients of wing rock equation
μ_x	=damping coefficient for sting bearing ($kg - m^4/s.$)
ρ	=density of air ($kg/m^3.$)
ρ^*	=positive constant
τ	=time constant (s.)
ϕ	=roll angle (rad.)
$\frac{\partial}{\partial \mathbf{x}}$	=partial derivative with respect to elements of $\mathbf{x}$
$\int[\,]dt$	=integration with respect to time
∞	=infinity
$\dot{()}$	=derivative with respect to time
$\ddot{()}$	=double derivative with respect to time
$[\,]^{-1}$	=inverse of the matrix

Chapter 1

INTRODUCTION

1.1 What is Wing Rock?

The term "wing rock" describes the motion of certain types of aircraft such as fighters, which operate at angles of attack, either near to stall onset, or when flow seperation effects are evident by aircraft buffeting. This type of motion has similarity to a lightly damped Dutch-Roll mode, except that the wing rock motion is a limit cycle oscillation. Compared to Dutch-Roll mode the amplitude of the wing rock motion is solely a result of aerodynamic nonlinearities, while the amplitude of the Dutch-Roll mode response is determined by the initial conditions.

Wing rock can also be described as lateral-directional instability for airplanes flying at high angles of attack. It is an uncommanded roll-yaw oscillation dominated by roll motion oscillating with a constant amplitude. It may be initiated either with a sideslip or during a zero-sideslip flight with some flow asymmetries over the aircraft flying at high angles of attack. Once the asymmetric flow starts, a roll-oscillation amplitude will keep building up if roll damping is negative. The transient amplitude of wing rock will grow gradually over some oscillation cycles because of instability and

negligible dihedral effect at low roll angle.

Although the roll damping is negative at small roll angles, it is positive at larger roll angles for a sustained wing rock. Both the effective dihedral effect and positive roll damping via aerodynamic nonlinearities at large roll angles will gradually reduce the roll rate. As these restoring moments become stronger, the aircraft will reach a threshold roll angle and finally switch the rolling direction. Thus, wing rock is constrained to a finite amplitude oscillation through nonlinear roll damping.

It occurs not only to low-aspect-ratio configurations, such as the F-4, F-5, F-14, X-29A, Gnat, Harrier, HP 115, and some re-entry vechicles, but also to high-aspect-ratio configurations, such as the Vari-Eze and some general aviation airplanes. Based on the extensive examination of available data, it can be concluded, as it has been done in Ref. [9], that wing rock is triggered by flow asymmetries, developed by negative roll damping, and sustained by nonlinear aerodynamic roll damping.

Wing rock oscillations provide major limitations on the low speed maneuvers of those aircrafts which have highly swept wing planforms. At certain flight conditions, such as short landing on carriers at high angles of attack, these oscillations can cause safety problems that must be taken into account while designing the aircraft control mechanism. Such mechanism can be established on the basis of some suitable mathematical model that is able to describe this highly nonlinear aerodynamic phenomenon as accurately as possible. The aerodynamic coefficients for this model can be obtained by measuring the forces acting on the aircraft, frequencies and their phase relation. On the other hand, in such experiments, these measurements are rather complex in nature because of the fact that the dynamic quantities involved are time dependent.

So, in order to get the required data, Nguyen et al. [1] have performed an experiment in which they have successfully recorded roll angle oscillations during self-induced wing rock of a flat plate delta wing with 80 deg leading edge sweep. From this, they have calculated the resulting rolling moments. In their experiment, the rolling axis of

free to roll model was mounted under the wing planform, resulting in a partial coning motion in addition to the pure roll oscillations.

In continuation with these experiments, Levin and Katz [2] have performed a similar experiment using two different models of aspect ratio 0.71 and 1.00. But this time their models have been mounted on a sting-balance apparatus and have been free to oscillate about their geometric axes, resulting in a pure roll oscillation. In addition to the roll angle, they have also measured normal and side forces and their phase relation. Theyhave conducted the testing of their models in two regimes, the static testing regime and the dynamic testing regime. They covered a wide range of angle of attack, angle of sideslip and roll angles to obtain the static test results. Based on these data, nonlinearities in the rolling moment slope have been detected. In the dynamic experiment, the wings have been mounted on a free to roll balance and the normal and side forces along with rolling angles have been then measured. Vortex patterns in the unsteady flow have been traced by helium-bubble flow visualisation, which have provided dynamic information about the vortex wake motion. This vortex wake motion plays an important role during the wing rock cycle.

In the above experiment, it has been observed that the narrower wing with aspect ratio 0.71 has exhibited self-induced roll oscillations while the wing with the aspect ratio of unity, which has higher damping in roll coefficient, does not exhibit wing rock motion. During the free-to-roll tests a loss in wing average lift, relative to the static lift, has been detected for the same angle of attack. Apart from this, the oscillation frequencies and their variations with wind tunnel speed and angle of attack, along with side force and normal force amplitudes, have been also recorded.

The two major questions in regard to this phenomenon are:
(1) What is the mechanism leading to the self induced oscillations?
(2) What is the reason for the reduction in the average normal force?
The explanation, as given in Ref. [2], based on the observed data is that these oscillations are sustained due to the momentarily reduced distance between the up-moving

semi-wing and leading-edge vortex originating from the same side. Thus, during the upward motion of this particular wing section a higher vortex suction force will result in a dynamic rolling moment, which is larger than the static value. This effect also causes the phase lag in the side force. On the other hand, vortex breakdown, has a damping effect on this motion, since flow visualisations have showed that the vortex burst is delayed relatively to the occurance of maximum roll angle. Furthermore, since under the dynamic conditions the wing upper surface is exposed to a more forward vortex breakdown, the average lift becomes less than the static value. In addition, during most of the roll cycle, only one leading edge vortex is present above the wing, whereas at the zero roll condition two of these vortices are present. Therefore, the reduction in the magnitude of the vortex lift, under the dynamic conditions, is obvious.

One significant difference between the two experiments has been that, whereas Ngyuen et al. [1] have measured no wing rock for their 80 deg delta wing below $\alpha = 27$ deg, Levin and Katz [2] have already measured wing rock at $\alpha = 20$ deg for the same leading edge sweep, where α is angle of attack. This early wing rock occurance is probably, as the authors [2] suggest, caused by the centrebody axis that has been used in their model. Also the sideslips of the two experiments were different.

Based on the information from these experimental results, Ericsson [3] has given an explanation of the underlying fluid mechanics leading to slender wing rock. According to him, two types of separation induced discontinuities occur for slender delta wing. One is caused by the leading edge vortices, for somewhat lesser slender delta wing. For very slender delta wings another type of discontinuity occurs before vortex breakdown, which is caused by asymmetric leading edge vortices. Vortex asymmetry occurs before vortex breakdown only for very slender delta wings.

Ericsson [3] has observed that wing rock starts before vortex breakdown, and as has been suggested earlier, wing rock is associated with a loss of time-average lift. It is due to the fact that the lift-off of one of the leading edge vortices will cause a loss of lift. Thus, he has concluded that wing rock is caused by the vortex asymmetry and not by

the vortex breakdown. He has explained the wing rock phenomenon in the following manner. At an $\alpha - \theta$ (apex half angle) combination where vortex asymmetry occurs, the wing half with the lifted-off vortex loses lift and dips down, rotating around the roll axis. As a result of increasing roll angle ϕ, the effective apex angle $\bar{\theta}$ is increased and the vortex attaches again. This produces a restoring rolling moment, the positive aerodynamic spring needed for the rigid body oscillation in roll. Due to the convective time lag effect Ref. [3], the wing is dynamically unstable in roll untill the amplitude has reached the limit cycle magnitude. At this magnitude the damping on both sides of the discontinuity balances the undamping.

Thus, the discontinuity which is introduced by the vortex asymmetry has all the characteristics that is needed for the limit cycle oscillation in roll. These characteristics, as he has observed, are lacking in vortex breakdown. If for some reason the vortex burst becomes asymmetric, the resulting net loss of lift on one wing half will cause it to "dip down". This increases ϕ and thereby θ, causing the wing half to penetrate further into the vortex burst region. No switch to a restoring moment occurs. The opposite wing half gets out of the vortex burst region, generating increased lift which adds to the statically destabilizing rolling moment. Thus vortex breakdown has aerodynamic characteristics leading to roll divergence which are completely opposite to those needed to cause slender wing rock. He also observed that the oscillations in roll damped down to zero amplitude if the 80-deg delta wing was yawed to $\gamma = 10$ deg at $\alpha = 27$ deg. This is due to the fact that windward wing half has $\bar{\theta} > 15$ deg leaving it outside of the boundary for asymmetric vortex shedding, whereas leeward wing half with $\bar{\theta} < 5$ deg remains inside the region for vortex asymmetry. Thus, neither wing half crosses the boundary and the wing-rock-inducing discontinuity is never encountered.

In addition to this, Ericsson et al. [4] have made an extensive study of the experimental results for advanced aircraft operating at high angles of attack. This has been quite helpful in understanding the phenomenon of wing rock further. They have observed that for aircraft with straight or moderately swept wings, wing rock occurs

first at moderate angles of attack. This type of wing rock is generated by the negative damping-in-plunge of the wing sections caused by dynamic airfoil stall. If the aircraft has long, slender nose, which often is the case, forebody vortices will generate wing rock at higher angles of attack where the wings are fully stalled. This type of wing rock has been observed in experiments with generic aircraft model, Ref. [4]. The flow mechanism causing the wing rock in this case is the downwash on the wing generated by forebody vortices. The X-29A aircraft experiences this type of forebody induced wing rock. When the inner portion of the wing has a highly swept leading edge, as in the cases of the F-18 HARV and X-31 aircraft, the high α wing rock is generated by direct interaction between the forebody vortices and the leading edge vortices from the inboard wing panels. Thus, from the above observations and a review of the available experimental results, Ericsson came to conclusion that wing rock of advanced aircraft will be driven by the vortices generated by forebody flow separation at high angle of attack, $\alpha > 30$ deg. The key flow phenomenon driving the forebody-induced wing rock is the coupling between forebody crossflow separation and vechicle motion. More precisely, the rolling moment generates moving wall effects, that control the cross flow separation on the forebody and the associated vortices provides the feedback mechanism responsible for the observed wing rock. The limit cycle oscillation results when this driving rolling moment generated by the forebody vortices is balanced by the roll damping generated by the stalling wing.

1.2 Mathematical Modelling of Wing Rock Motion

After getting a good grasp of the wing rock phenomenon, now we proceed to analyse briefly the various valuable contributions of different scholars made in this field.

Ross [5] has made a combined experimental and theoretical study of the nonlinear lateral oscillation experienced by a slender-wing aircraft at high angles of attack. Flight tests of HP 115 research aircraft have confirmed the expectation that the Dutch-

Roll oscillation is undamped at high angles of attack, and has also showed that the limit cycle develops, with steady amplitude at bank angle of about 30 deg. He has measured the stability derivatives along with the responses that has been obtained from the RAE flight dynamics simulater. From the digital computation of the equations of motion, he has observed that a wing rock limit cycle can exist when the nonlinearity is a cubic behaviour in either yawing or rolling moment with respect to the side slip angle. He has used the method of slowly varying parameters in order to demonstrate the limit cycle. In this method, the cross coupled nonlinear differential equations are reorganised into a single, high order differential equation, and the influence of nonlinear aerodynamic coefficients are analysed by stability criteria.

An analysis is presented by Schmidt [6] using control theory concepts to show that aerodynamic hysteresis of the form of relay action can lead to lateral directional limit cycle motion. His analysis is an application of control theory, where the cross-coupled second order differential equations are cast into state variable form to yield a larger set of first order differential equations. This system is convenient for linear system analysis and quite adaptable to hysteresis situations from relay type inputs. The advantage of this technique is that physical concepts or principles become understandable and a broader insight is acquired. From his analysis, Schmidt [6] has made the following observations.

(1) Limit cycle period does not differ significantly from the Dutch-Roll period, and does not change with the magnitude of roll moment hysteresis.

(2) The limit cycle amplitudes are directly related to the magnitude of the roll moment relay action.

(3) The sign of roll hysteresis parameter during switching can be determined from the requirement that a limit cycle with a dissipative system requires extraction of energy from the free stream.

(4) During a limit cycle, the first harmonic of the roll rate response is approximately in phase with the sideslip angle rate while it is approximately 90 deg out of phase during a Dutch-Roll oscillation.

(5) In addition to the phase differences between the limit cycle and Dutch-Roll oscil-

lations, the relative amplitude ratios of bank angle to sideslip angle are different, for example, the ratio during limit cycle being about 8.5 times greater than that occuring during a Dutch-Roll oscillations.

From the results of the experiments of References [1] and [2], a numerical simulation of these wind tunnel experiments has been developed by Konstadinopoulos et al.[7]. They have used unsteady vortex-lattice method to obtain aerodynamic loads and the equations governing wing rock motion have been integrated by a predictor-corrector scheme. The solution provides complete information about the motion of the wing and the flowfield simultaneously, fully accounting for dynamic-aerodynamic interaction. Their simulation predicts that the symmetric configuration of the leading-edge vortex becomes unstable as the angle of attack increases. This causes a loss of roll damping at small angles of roll. Consequently, small disturbances which are introduced into the flowfield grow, causing wing rock to develop. Also, from their simulation an analytic expression for roll moment can be developed, which is a third order polynomial in roll angle and roll rate that fits the numerical data extremely well from the start of the motion to the development of limit cycles or decay depending on the angle of attack. The model simulates hysteresis, aerodynamic damping and leading edge separation. It is not limited by angle of attack, twist, camber, or planform as long as vortex bursting does not occur in the near vicinity of the wing.

Their numerical simulation predicts onset angles as well as the periods and amplitudes of the limit cycles in close agreement with the two experiments. Moreover, the simulation shows that the symmetric arrangement of the leading-edge-vortex system at zero roll becomes unstable. This asymmetry causes a roll moment to develop. But as the angle of roll increases, the change in the apparent direction of the free stream causes the direction of the moment and eventually, the direction of rotation to change.

The aforesaid expression for roll moment has been substituted in the equation of motion by Nayfeh et al. [8] Thus, they have obtained a five term, third order polynomial in roll angle and roll rate. They have used this polynomial to construct

phase planes that show the locations of equilibrium positions, limit cycles, and domain of initial conditions that lead to the different possible motions. In addition to this, the use of this polynomial in the equation of motion makes it possible to obtain assymptotic approximations to the expressions for limit-cycle amplitudes and periods.

Hsu and Lan [9] have developed another nonlinear aerodynamic model to investigate the main aerodynamic nonlinearities causing wing rock. They have solved the resulting nonlinear flight dynamics equations of both one and three degrees of freedom with the help of Beecham-Titchener asymptotic method for the limit cycle amplitude and wing rock frequency. The latter are calculated iteratively in combination with a nonlinear aerodynamic method. Theoretical results of their model show that to sustain a steady state wing rock, the total aerodynamic roll damping must be negative at small bank angles. On the other hand, at large bank angles it must be positive.

1.3 Control of Wing Rock

There are three possible approaches to supress or prevent wing rock:
(1) The first approach involves attaining the wing rock free capability through a detailed aerodynamic reshaping of the basic airframe configuration.
(2) The second approach introduces maneuver limiting by addopting an alpha limiter, however, this approach degrades maneuverability.
(3) The third approach employs stability augmented systems (SAS) or automatic flight control systems. These have become the most effective methods for attaining strong resistance to wing rock without degrading maneuverability.

Luo and Lan [10] have presented a theoretical analysis to determine the optimal control input for wing rock suppression through a Hamiltonian formulation. The optimality equations are analysed through Beecham- Titchener's averaging technique and are numerically integrated by a backward differentiation formulas method. They have shown that the weighting factors in the cost function is related explicitly to the

system output damping and frequency. They have also shown that an effective way to suppress wing rock is to control the roll rate. System sensitivity is investigated by determining variations in system output damping and frequency with aerodynamic model coefficients. The results show that higher sensitivity corresponds to lower system damping.

Monahemi and Krstic [11] have applied the theory of adaptive control of feedback linearizable systems for designing the control of wing rock motion with the extension of technique to include tracking. The adaptive regulation and tracking is achieved using a recursive design procedure known as backstepping with tuning functions. The procedure is such that at each step the subsystem is stabilised with respect to a Lyapunov function by designing an appropriate tuning function. At the final step one develops the feedback control and the update law for the parameter estimates. The designed control and parameter update laws can track a prespecified model system with remarkable accuracy reaching steady state within a transient stage of any desired time length. Thus, without any degradation the required maneuvers can be maintained simultaneously with the suppression of wing rock. Such a performance requires the availability of sufficient rolling moment because of the lateral control. The design proceedure accomodates aerodynamic parameter estimation and updates online while the control system is in operation.

Singh et al. [12] have employed an adaptive and neural control of the wing rock motion. Neural networks have architecture that has massively parallel interconnections of simple "neural" processors. These networks have ability to "learn" a mapping between an input space and an output space. In this approach, however, the control cancels the nonlinearity of the main equation (the roll moment equation) only in a very limited sense, i.e., there exists no additional dynamics and/ or an actuater control surface equation.

Adaptive control systems developed in Refs. [11] and [12] assume that the wing rock model does not have disturbance input and that the structure of nonlinear func-

tions, except for the neural control, is known. In the presence of the external disturbance inputs and unmodeled nonlinearities, adaption laws of internal type used in Refs. [11] and [12] can cause divergence of controller parameters.

Araujo and Singh [13] have designed a control system for the control of wing rock motion of simple slender delta wings which is based on the theory of variable structure model reference adaptive control (VS-MRAC), using only input and output signals. Their wing rock model can include disturbance input and unstructured nonlinear aerodynamic functions. In Ref. [13] only roll angle measurement is required for controller synthesis. For the derivation of the control law, it is assumed that the aerodynamic parameters and the structure of the nonlinear functions in the model are unknown. Moreover, it is assumed that the disturbance input due to wind gust is present in the system. Ref. [13] have shown that, in the closed loop system, the roll angle tracks a given reference trajectory, and wing rock suppression is accomplished.

Shue et al. [14] have presented a procedure for optimising a state feedback control law for a nonlinear system with respect to a positive performance index. They have employed Hamilton-Jacobi-Bellman equation to derive the optimality equations wherein this performance index is minimised. The closed loop Lyapunov function is assumed to have the same matrix form of state variables as the performance index. The constants of these matrices are easily determined so as to guarantee their positive definitenesses. The optimal nonlinear system is asymptotically stable in the large, as both the closed loop Lyapunov function and performance index are positive definite. It is also shown that the wing rock model using nonlinear state feedback is asymptotically stable in the large. Both optimal linear and nonlinear state feedback cases are evaluated. Even though the major emphasis is placed on the second order system in their paper, the procedure is applicable to any system of finite order. It is this procedure, which has been utilised in this thesis, to obtain the optimal feedback control for wing rock problem along with some modifications like considering an actuator and sideslip effects, which have been neglected in Ref. [14].

Chapter 2

METHODOLOGY

2.1 Modelling of the Wing Rock Motion

Currently there are several theoretical models proposed to describe wing rocking. Each model has been variefied only for a particular configuration. In fact, none of the models can predict the amplitude and period of wing rock motion for all configurations.

In this thesis, the models developed in Refs. [8] and [12] have been used.The equations of motion of the two References are compared here in order to get an idea of the variables on which the coefficients, used in Ref. [8] depend. Rate of change of angular momentum gives the following equations:

$$L = I_x \dot{p} \tag{2.1}$$

or

$$\dot{p} = \frac{L}{I_x} \tag{2.2}$$

where p is the roll rate, L is the rolling moment and I_x is the roll moment of inertia. Also from Ref. [12] we have

$$\dot{p} = \frac{qSb}{I_x}[C_{l\beta}(\alpha)\beta sin\alpha + C_{lp}(\alpha,\beta)(pb/2V)] \tag{2.3}$$

where q, S, b and V are the dynamic pressure, wing reference area, wing span and freestream air velocity respectively. The coefficient $C_{l\beta}$ is the rolling moment stability derivative because of sideslip angle β and the coefficient C_{lp} is the rolling moment derivative because of roll rate p. On comparing Eqs. (2.2) and (2.3) we get

$$L = qSb[C_{l\beta}(\alpha)\beta sin\alpha + C_{lp}(\alpha,\beta)(pb/2V)] \tag{2.4}$$

Now, rolling moment L depends on sideslip angle β and roll rate p. Therefore L can be written as

$$L = L_\beta \beta + L_p p \tag{2.5}$$

where L_β and L_p are rolling moment due to sideslip angle and roll rate respectively. On comparing Eqs. (2.4) and (2.5) we get,

$$L_\beta = qSbC_{l\beta}(\alpha)sin\alpha \tag{2.6}$$

$$L_p = qSbC_{lp}(\alpha,\beta)(pb/2V) \tag{2.7}$$

Thus, we can write

$$\dot{p} = \frac{L_\beta}{I_x}\beta + \frac{L_p}{I_x}p \tag{2.8}$$

The equation of motion used in Ref. [8] is

$$\ddot{\phi} = C_1 C_l - C_2\dot{\phi} \tag{2.9}$$

where ϕ is the roll angle and C_l is the aerodynamic roll-moment coefficient.

$$\dot{\phi} = p \tag{2.10}$$

$$C_1 = \rho S c L_c^2/2I_x \tag{2.11}$$

$$C_2 = \mu_x L_c/I_x U_c \tag{2.12}$$

where ρ is the density of the air, c the chord, L the characteristic length, μ_x the damping coefficient for the sting bearing and U_c is the characteristic speed. The dot in Eq. (2.9) implies that the derivative is with respect to the non-dimensional time

$$t^* = (U_c/L_c)t \tag{2.13}$$

On comparing Eqs. (2.8) and (2.9) we get

$$C_2 = -\frac{qSb}{I_x} C_{lp}(\alpha, \beta) b/2V \tag{2.14}$$

and from Eqs. (2.12) and (2.13) we find that

$$\mu_x = -qSbC_{lp}(\alpha, \beta)/2 \tag{2.15}$$

Again on comparing Eqs. (2.8) and (2.9) we get

$$C_1 C_l = \frac{qSb}{I_x} C_{l\beta}(\alpha) \beta sin\alpha \tag{2.16}$$

where,

$$q = \frac{1}{2}\rho V^2 \tag{2.17}$$

Thus, on substituting the expression for q and C_1 in Eq. (2.16) we get

$$\frac{\rho S c L_c^2}{2I_x} C_l = \frac{\rho V^2 Sb}{2I_x} C_{l\beta}(\alpha) \beta sin\alpha \tag{2.18}$$

On simplification we get

$$C_l = \frac{V^2}{cb} C_{l\beta}(\alpha) \beta sin\alpha \tag{2.19}$$

The expression for C_l used in Ref. [8] is

$$C_l = a_1\phi + a_2\dot{\phi} + a_3\dot{\phi}^3 + a_4\phi^2\dot{\phi} + a_5\phi\dot{\phi}^2 \tag{2.20}$$

The value of a_i depend on the angle of attack, as it can be observed from Eq. (2.19). They are given in Table (1). Eq. (2.20) fits the calculated moment through the transients and into the regime where steady state motion exists. This form for C_l has evolved from a much more general beginning, which included a total 12 terms in a fifth order polynomial. Seven of these terms have been systematically eliminated because of their small contributions.

Substitution of Eq. (2.20) into Eq. (2.9) leads to

$$\ddot{\phi} + \omega^2\phi = \mu_1\dot{\phi} + b_1\dot{\phi}^3 + \mu_2\phi^2\dot{\phi} + b_2\phi\dot{\phi}^2 \tag{2.21}$$

where,

$$\omega^2 = -C_1 a_1 \tag{2.22}$$

$$\mu_1 = C_1 a_2 - C_2 \tag{2.23}$$

$$b_1 = C_1 a_3 \tag{2.24}$$

$$\mu_2 = C_1 a_4 \tag{2.25}$$

$$b_2 = C_1 a_5 \tag{2.26}$$

The point where μ_1 is zero corresponds to the onset of wing rock.

Table 1. Coefficients in the analytical expression for the roll moment, at different angles of attack

α	a_1	a_2	a_3	a_4	a_5
15	-0.01026	-0.02117	-0.14181	0.99735	-0.83478
21.5	-0.04207	0.01456	0.04714	-0.18583	0.24234
22.5	-0.04681	0.01966	0.05671	-0.22691	0.59065
25	-0.05686	0.03254	0.07334	-0.3597	1.4681

Now we have reached at a stage where we must seek some approriate procedure to solve the above mentioned equation of motion, so that we may be able to observe the type of motion which the aircraft is executing, and latter develop some control system to control the undesirable motion.

2.2 Control of Wing Rock Motion

Before developing some procedure to solve our equation of motion obtained in the previous section, let us have a brief understanding of the control systems. The basic control system problem may be described by the simple block diagram shown in Fig. (3.1). The main objective of the system is to control the variable c in some prescribed manner by an acuating signal e through the elements of controlled process.

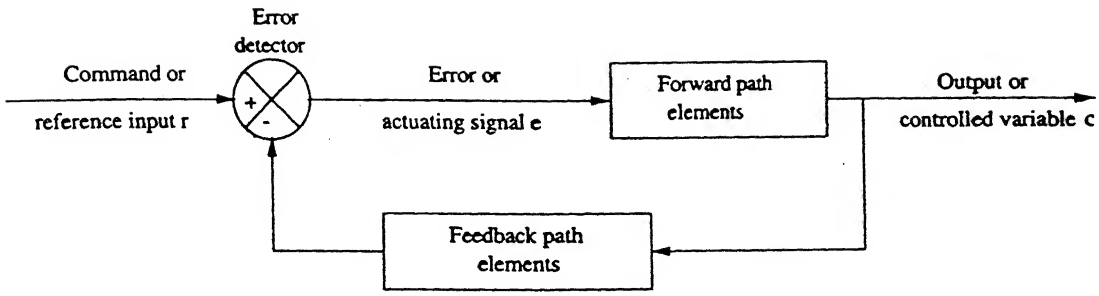

Figure 2.1: Basic block diagram of a feedback control system

Control systems may be classified into two types depending on whether the controlled variable affects the actual input to the control system or not, i.e., whether some kind of feedback is used or not. When feedback is not used, the system is called an open loop system, when used, it is called a closed loop system.

In an open loop system an input known as reference input is applied directly to the controller, and an output known as controlled output is obtained. Here in an open loop system the input to the controller is in no way affected by the value of the controlled output. Also, this type of system do not adapt to the variations in environmental conditions or to external disturbances.

What is missing in the open loop control system for more accurate control is a link or feedback path between the output and the input of the system. In order to obtain more accurate control, the controlled signal must be fed and compared with the command or reference input, and an actuating signal proportional to the difference of the output and the input must be sent through the system to correct the error. A system with a feedback path is called a closed loop system.

The analysis and design of feedback control systems are usually carried out by using either linear or nonlinear techniques. Strictly speaking, linear systems do not exist in practice, since all physical systems are nonlinear to some extent. Therefore, linear feedback control systems are idealized systems. When the magnitudes of the actuating signals are limited to a range in which system components are considered linear, these components may be represented by their linear models and counterparts.

But when the actuating signals are extended outside the range of linear operations, the feedback control systems become nonlinear.

We can now proceed forward to solve our equation of motion, under these two headings.

2.2.1 The Open Loop System

The equation of motion of the aircraft is

$$\ddot{\phi} + \omega^2\phi = \mu_1\dot{\phi} + b_1\dot{\phi}^3 + \mu_2\phi^2\dot{\phi} + b_2\phi\dot{\phi}^2 \tag{2.27}$$

The above second order equation can be written as a system of two first order equations.

$$\dot{x_1} = x_2 \tag{2.28}$$

$$\dot{x_1} = \dot{x_2} = -\omega^2 x_1 + \mu_1 x_2 + b_1 x_2^3 + \mu_2 x_1^2 x_2 + b_2 x_1 x_2^2 \tag{2.29}$$

where

$$x_1 = \phi \tag{2.30}$$

To find the equilibrium positions, we substitute

$$\dot{x_1} = \dot{x_2} = 0 \tag{2.31}$$

From this, it follows that

$$x_1 = 0, \pm\omega/\sqrt{b_1} \tag{2.32}$$

The nonzero solution exists only when b_1 is greater than zero. It is observed that b_1 and μ_1 change sign at the same angle of attack,Ref. [8]. At the angle of attack when b_1 is zero, two of these equilibrium positions are at infinity. As the angle of attack increases, these two point move towards the origin.

2.2.2 The Closed Loop System

Flight at high angle of attack, the exhibition of limit cycle behaviour of the motion variables, and the creation of large amplitudes for the motion variables lead to severe requirements for the flight control system that cannot be met using conventional procedures. Nonlinear properties are essential features of the aircraft dynamics in these regimes. Techniques that are needed must be

(1) computationally feasible,

(2) retain the nonlinearities inherent within the vechicle dynamics,

(3) provide physical and mathematical understanding of the important flying qualities.

Thus, keeping the above factors in mind, the same procedure which has been used in Ref. [15], has been utilised in this thesis for optimizing a state feedback control law for our nonlinear system with respect to a positive performance index. Here also, the Hamilton-Jacobi-Bellman equation is used to derive the optimality equations so that this performance index is minimised.

Let us consider a vector-matrix linear differential equation

$$\dot{\mathbf{x}} = \mathbf{A}\mathbf{x} + \mathbf{B}\mathbf{u} \tag{2.33}$$

where $\mathbf{x}$ is the process state, $\mathbf{u}$ is the control input, and $\mathbf{A}$ and $\mathbf{B}$ are known matrices. We now seek a procedure to minimise a specified performance index (or cost function) expressed as the integral of a quadratic form in the state x plus a second quadratic form in the control $\mathbf{u}$; i.e.,

$$J = \int_t^{T^*} [\mathbf{x}^T\mathbf{Q}\mathbf{x} + \mathbf{u}^T\mathbf{R}\mathbf{u}]dt \tag{2.34}$$

where $\mathbf{Q}$ and $\mathbf{R}$ are symmetric matrices. Let us talk about this performance index in brief, before we attempt to find the optimum solution.

First, we note that minimization of J also minimizes $\rho^* J$ where ρ^* is any positive constant. So the problem is not altered by multiplying J by any positive constant. Often the constant $1/2$ is used in front of J to simplify expressions resulting in other developements.

Second, regarding the limits on the integral, the lower limit t is identified as the present time, and the upper limit T^* is the terminal time, or final time. The time difference $T^* - t$ is the control interval, or "time to go". In our case, the terminal time is infinite. Here, we are interested in the behaviour of the process "from now on", including the steady state.

Finally, consider the weighting matrices $\mathbf{Q}$ and $\mathbf{R}$. These are called the state weighting matrix and the control weighting matrix, respectively. The question of concern to the control system designer is the selection of the weighting matrices $\mathbf{Q}$ and $\mathbf{R}$.

In the performance or cost function defined as above, two terms contribute to the integrated cost of control: the quadratic form $\mathbf{x}^T\mathbf{Q}\mathbf{x}$ which represents a penalty on the deviation of the state $\mathbf{x}$ from the origin and the term $\mathbf{u}^T\mathbf{R}\mathbf{u}$ which represents the "cost of control". This means that the desired state is the origin and not some other state. The weighting matrix $\mathbf{Q}$ specifies the importance of the various components of the state vector relative to each other. The term $\mathbf{u}^T\mathbf{R}\mathbf{u}$ in the performance index is included in an attempt to limit the magnitude of the control signal $\mathbf{u}$. Unless a "cost" is imposed for the use of control, the design that emerges is liable to generate control signals that cannot be achieved by the actuator and the result will be that the control signal will saturate at the maximum signal that can be produced.

The above type of problem where performance index is of a quadratic form and the system is linear one, is known as linear quadratic regulator (LQR) problem. The Hamilton-Jacobi-Bellman (HJB) equation is

$$H = \frac{1}{2}\mathbf{x}^T\mathbf{Q}\mathbf{x} + \frac{1}{2}\mathbf{u}^T\mathbf{R}\mathbf{u} + \frac{\partial V(\mathbf{x})}{\partial \mathbf{x}}\dot{\mathbf{x}} \tag{2.35}$$

where $V(\mathbf{x})$ is the Lyapunov function and $\frac{\partial}{\partial \mathbf{x}}$ denotes the derivative with respect to elements of $\mathbf{x}$.

Earlier, the (HJB) equation has been applied in solving (LQR) problems. LQR is guaranteed to have an optimal and asymptotically stable solution because the closed

loop Lyapunov function is positive definite or positive semi-definite and its time derivative is negative.

For the extension of the LQR problem to the nonlinear optimal control problem, the following conditions must be satisfied.

Condition 1:

$$V(\mathbf{x}) \geq 0, \qquad V(\mathbf{0}) = 0 \tag{2.36}$$

Condition 2:

$$min\{H\} = min\left\{\frac{1}{2}\mathbf{x}^T\mathbf{Q}\mathbf{x} + \frac{1}{2}\mathbf{u}^T\mathbf{R}\mathbf{u} + \frac{\partial V(\mathbf{x})}{\partial \mathbf{x}}\dot{\mathbf{x}}\right\} = 0 \tag{2.37}$$

Condition 3:

$$\mathbf{x}^T\mathbf{Q}\mathbf{x} \geq 0 \tag{2.38}$$

From condition 2 we can find that

$$\dot{V}(\mathbf{x}) = \frac{\partial V(\mathbf{x})}{\partial \mathbf{x}}\dot{\mathbf{x}} = -\frac{1}{2}[\mathbf{x}^T\mathbf{Q}\mathbf{x} + \mathbf{u}^T\mathbf{R}\mathbf{u}] \leq 0 \tag{2.39}$$

if condition 3 is satisfied.

In fact, no matter whether or not the linear system or nonlinear system uses nonlinear feedback control, the system's closed loop Lyapunov function has to be positive definite. As with the LQR problem, the performance index plays a very important role in the problem of optimal control of nonlinear systems. When a positive definite Lyapunov function cannot be found, this purpose usually can be achieved through changing the cost function.

In this thesis, a procedure is employed that produces a closed loop Lyapunov function and a performance index that are positive definite, and the HJB equation is also satisfied. This means that the system is asymptotically stable in the large.

Consider a time invarient nonlinear system

$$\dot{\mathbf{x}} = \mathbf{A}\mathbf{x} + \mathbf{F}(\mathbf{x}) + \mathbf{B}\mathbf{u} \tag{2.40}$$

where $\mathbf{A}$, $\mathbf{B}$, $\mathbf{x}$, $\mathbf{u}$ have already been stated, and $\mathbf{F}(\mathbf{x})$ represents the higher order term with respect to the state variable $\mathbf{x}$. Therefore, $f(\mathbf{x})$ which is an element of $\mathbf{F}(\mathbf{x})$, may be written in the following form:

$$f(\mathbf{x}) = f_2(\mathbf{x}) + f_3(\mathbf{x}) + \cdots + f_{2n-1}(\mathbf{x}); \qquad n \geq 2 \tag{2.41}$$

Note that the subscripts of $f(\mathbf{x})$, the performance index, the closed loop Lyapunov function, and the Hamiltonian matrix represent the order of the state variable $\mathbf{x}$. We can define a performance index

$$J = \frac{1}{2}\int_0^\infty [q(\mathbf{x}) + \mathbf{u}^T\mathbf{R}\mathbf{u}]dt \tag{2.42}$$

where

$$q(\mathbf{x}) = \begin{bmatrix} \mathbf{x} \\ \mathbf{x}^2 \\ \vdots \\ \mathbf{x}^n \end{bmatrix}^T \begin{bmatrix} \mathbf{Q}_{1,1} & \mathbf{Q}_{1,2} & \cdots & \mathbf{Q}_{1,n} \\ \mathbf{Q}_{2,1} & \mathbf{Q}_{2,2} & \cdots & \mathbf{Q}_{2,n} \\ \vdots & \vdots & \ddots & \vdots \\ \mathbf{Q}_{n,1} & \mathbf{Q}_{n,2} & \cdots & \mathbf{Q}_{n,n} \end{bmatrix} \begin{bmatrix} \mathbf{x} \\ \mathbf{x}^2 \\ \vdots \\ \mathbf{x}^n \end{bmatrix} \tag{2.43}$$

with $q(\mathbf{x})\geq 0$, and $\mathbf{Q_{i,j}} = \mathbf{Q_{j,i}}$ when $i \neq j$. Also, $\mathbf{R}$ is assumed to be symmetric, orthogonal, and positive definite matrix. Therefore,

$$q(\mathbf{x}) = q_2(\mathbf{x}) + q_3(\mathbf{x}) + \cdots + q_{2n}(\mathbf{x}) \tag{2.44}$$

where

$$\begin{gathered} q_2(\mathbf{x}) = \mathbf{x}^T\mathbf{Q}_{1,1}\mathbf{x} \\ q_3(\mathbf{x}) = \mathbf{x}^T\mathbf{Q}_{1,2}\mathbf{x}^2 + (\mathbf{x}^2)^T\mathbf{Q}_{2,1}\mathbf{x} \\ q_4(\mathbf{x}) = \mathbf{x}^T\mathbf{Q}_{1,3}\mathbf{x}^3 + (\mathbf{x}^2)^T\mathbf{Q}_{2,2}\mathbf{x}^2 + (\mathbf{x}^3)^T\mathbf{Q}_{3,1}\mathbf{x} \\ \vdots \quad \vdots \quad \vdots \\ q_{2n}(\mathbf{x}) = (\mathbf{x}^n)^T\mathbf{Q}_{n,n}\mathbf{x}^n \end{gathered}$$

The optimal control problem of the system in Eq. (2.40) is to find the state feedback gain

$$\mathbf{u} = \mathbf{u}(\mathbf{x}) \tag{2.45}$$

such that the performance index is minimised. The HJB equation is applied to find the optimal solution of the system,

$$H = \frac{1}{2}q(\mathbf{x}) + \frac{1}{2}\mathbf{u}^T\mathbf{R}\mathbf{u} + \frac{\partial V(\mathbf{x})}{\partial \mathbf{x}}[\mathbf{A}\mathbf{x} + \mathbf{F}(\mathbf{x}) + \mathbf{B}\mathbf{u}] = 0 \tag{2.46}$$

where

$$\frac{\partial V(\mathbf{x})}{\partial \mathbf{x}} = \left[\frac{\partial V(\mathbf{x})}{\partial x_1}, \frac{\partial V(\mathbf{x})}{\partial x_2}, \cdots, \frac{\partial V(\mathbf{x})}{\partial x_n}\right] \tag{2.47}$$

For optimal control,

$$\frac{\partial H}{\partial \mathbf{u}} = 0 \tag{2.48}$$

Thus on solving the above equation, we obtain the optimal control as

$$\mathbf{u}(\mathbf{x}) = -\mathbf{R}^{-1}\mathbf{B}^T\left[\frac{\partial V(\mathbf{x})}{\partial \mathbf{x}}\right]^T \tag{2.49}$$

On substituting Eq. (2.49) into Eq. (2.46) we get

$$H = \frac{1}{2}q(\mathbf{x}) - \frac{1}{2}\frac{\partial V(\mathbf{x})}{\partial \mathbf{x}}\mathbf{B}\mathbf{R}^{-1}\mathbf{B}^T\left[\frac{\partial V(\mathbf{x})}{\partial \mathbf{x}}\right]^T + \frac{\partial V(\mathbf{x})}{\partial \mathbf{x}}[\mathbf{A}\mathbf{x} + \mathbf{F}(\mathbf{x})] = 0 \tag{2.50}$$

It is assumed that the Lyapunov function has the same form as the cost function (J),

$$V(\mathbf{x}) = \frac{1}{2}\begin{bmatrix} \mathbf{x} \\ \mathbf{x}^2 \\ \vdots \\ \mathbf{x}^n \end{bmatrix}^T \begin{bmatrix} \mathbf{P}_{1,1} & \mathbf{P}_{1,2} & \cdots & \mathbf{P}_{1,n} \\ \mathbf{P}_{2,1} & \mathbf{P}_{2,2} & \cdots & \mathbf{P}_{2,n} \\ \vdots & \vdots & \ddots & \vdots \\ \mathbf{P}_{n,1} & \mathbf{P}_{n,2} & \cdots & \mathbf{P}_{n,n} \end{bmatrix} \begin{bmatrix} \mathbf{x} \\ \mathbf{x}^2 \\ \vdots \\ \mathbf{x}^n \end{bmatrix} \tag{2.51}$$

and $V(\mathbf{x}) \geq 0$, where $\mathbf{P}_{i,j} = \mathbf{P}_{j,i}$ when $i \neq j$. therefore,

$$V(\mathbf{x}) = V_2(\mathbf{x}) + V_3(\mathbf{x}) + \cdots + V_{2n}(\mathbf{x}) \tag{2.52}$$

where

$$V_2(\mathbf{x}) = \tfrac{1}{2}\mathbf{x}^T\mathbf{P}_{1,1}\mathbf{x}$$
$$V_3(\mathbf{x}) = \tfrac{1}{2}\mathbf{x}^T\mathbf{P}_{1,2}\mathbf{x}^2 + \tfrac{1}{2}(\mathbf{x}^2)^T\mathbf{P}_{2,1}\mathbf{x}$$
$$\vdots \quad \vdots \quad \vdots$$
$$V_{2n}(\mathbf{x}) = \tfrac{1}{2}(\mathbf{x}^n)^T\mathbf{P}_{n,n}\mathbf{x}^n$$

Note that the performance index and the Lyapunov function are symmetric.

Let

$$H = H_2 + H_3^* + H_4 + \cdots + H_{2n} \tag{2.53}$$

Substituting Eqs. (2.41), (2.43), and (2.51) into Eq. (2.50) and rearranging based on the order of the state variable, we get

$$H_2 = \frac{1}{2}q_2(\mathbf{x}) - \frac{1}{2}\frac{\partial V_2(\mathbf{x})}{\partial \mathbf{x}}\mathbf{B}\mathbf{R}^{-1}\mathbf{B}^T\left[\frac{\partial V_2(\mathbf{x})}{\partial \mathbf{x}}\right]^T + \frac{\partial V_2(\mathbf{x})}{\partial \mathbf{x}}\mathbf{A}\mathbf{x} = 0 \tag{2.54}$$

$$H_3 = \frac{1}{2}q_3(\mathbf{x}) - \frac{1}{2}\frac{\partial V_2(\mathbf{x})}{\partial \mathbf{x}}\mathbf{B}\mathbf{R}^{-1}\mathbf{B}^T\left[\frac{\partial V_3(\mathbf{x})}{\partial \mathbf{x}}\right]^T$$
$$-\frac{1}{2}\frac{\partial V_3(\mathbf{x})}{\partial \mathbf{x}}\mathbf{B}\mathbf{R}^{-1}\mathbf{B}^T\left[\frac{\partial V_2(\mathbf{x})}{\partial \mathbf{x}}\right]^T + \frac{\partial V_3(\mathbf{x})}{\partial \mathbf{x}}\mathbf{A}\mathbf{x} + \frac{\partial V_2(\mathbf{x})}{\partial \mathbf{x}}f_2(\mathbf{x}) = 0 \quad (2.55)$$

$$H_4 = \frac{1}{2}q_4(\mathbf{x}) - \frac{1}{2}\frac{\partial V_2(\mathbf{x})}{\partial \mathbf{x}}\mathbf{B}\mathbf{R}^{-1}\mathbf{B}^T\left[\frac{\partial V_4(\mathbf{x})}{\partial \mathbf{x}}\right]^T$$
$$-\frac{1}{2}\frac{\partial V_3(\mathbf{x})}{\partial \mathbf{x}}\mathbf{B}\mathbf{R}^{-1}\mathbf{B}^T\left[\frac{\partial V_3(\mathbf{x})}{\partial \mathbf{x}}\right]^T - \frac{1}{2}\frac{\partial V_4(\mathbf{x})}{\partial \mathbf{x}}\mathbf{B}\mathbf{R}^{-1}\mathbf{B}^T\left[\frac{\partial V_2(\mathbf{x})}{\partial \mathbf{x}}\right]^T$$
$$+\frac{\partial V_4(\mathbf{x})}{\partial \mathbf{x}}\mathbf{A}\mathbf{x} + \frac{\partial V_3(\mathbf{x})}{\partial \mathbf{x}}f_2(\mathbf{x}) + \frac{\partial V_2(\mathbf{x})}{\partial \mathbf{x}}f_3(\mathbf{x}) = 0 \quad (2.56)$$

$$\vdots \quad \vdots \quad \vdots$$

$$H_{2n} = \frac{1}{2}q_{2n}(\mathbf{x}) - \frac{1}{2}\frac{\partial V_2(\mathbf{x})}{\partial \mathbf{x}}\mathbf{B}\mathbf{R}^{-1}\mathbf{B}^T\left[\frac{\partial V_{2n}(\mathbf{x})}{\partial \mathbf{x}}\right]^T$$
$$-\cdots-\frac{1}{2}\frac{\partial V_{2n}(\mathbf{x})}{\partial \mathbf{x}}\mathbf{B}\mathbf{R}^{-1}\mathbf{B}^T\left[\frac{\partial V_2(\mathbf{x})}{\partial \mathbf{x}}\right]^T + \frac{\partial V_{2n}(\mathbf{x})}{\partial \mathbf{x}}\mathbf{A}\mathbf{x}$$
$$+\frac{\partial V_{2n-1}(\mathbf{x})}{\partial \mathbf{x}}f_2(\mathbf{x}) + \cdots + \frac{\partial V_2(\mathbf{x})}{\partial \mathbf{x}}f_{2n-1}(\mathbf{x}) = 0 \quad (2.57)$$

Solving Eq. (2.54), the algebraic Riccati equation is obtained,

$$\mathbf{A}^T\mathbf{P}_{1,1} + \mathbf{P}_{1,1}\mathbf{A} + \mathbf{Q}_{1,1} - \mathbf{P}_{1,1}\mathbf{B}\mathbf{R}^{-1}\mathbf{B}^T\mathbf{P}_{1,1} = 0 \quad (2.58)$$

Solving the algebraic Riccati equation, and substituting $\mathbf{P_{1,1}}$ back into Eq. (2.55), $\mathbf{P_{2,1}}$ can be found. The remaining values of the Lyapunov matrix can be found by successive substitution of the lower order Lyapunov parameters into higher order Lyapunov parameters until $\mathbf{P_{n,n}}$ is found. After all Lyapunov parameters have been determined, stability of the Lyapunov function has to be checked: if $V(\mathbf{x}) > 0$ and $q(\mathbf{x}) > 0$, then the nonlinear optimal control is asymptotically stable in the large.

2.2.3 Nonlinear Optimal Control Procedure

The general procedure for solving the Lyapunov function V(x) is as follows.

Step 1: Find the highest order (2n-1) of the state variable from the state equation, so

that n can be properly selected.

Step 2: Assume q(x) and V(x) have the form of Eqs. (2.43) and (2.51) respectively.

Step 3: Solve the algebraic Riccati equation from Eq. (2.58) and differentiate $V_2(\mathbf{x})$ and $V_3(\mathbf{x})$ with respect to x to find $\partial V_2(\mathbf{x})/\partial \mathbf{x}$ and $\partial V_3(\mathbf{x})/\partial \mathbf{x}$.

Step 4: Substitute $\partial V_2(\mathbf{x})/\partial \mathbf{x}$ and $\partial V_3(\mathbf{x})/\partial \mathbf{x}$ into Eq. (2.55) and solve it to obtain the values of matrix $\mathbf{P_{2,1}}$.

Step 5: Check the positive definiteness of the Lyapunov function. If it is not stable, then adjust the performance index and repeat step 4.

Step 6: Repeat the process until $V_{2n}(\mathbf{x})$ is determined.

The outline procedure will always result in a positive definite V(x). Note that for stability $V_n(\mathbf{x})$ has to be positive definite.

Feedback Using Instantaneous Control

Now we are in a position to apply the above methodology to our problem and solve the equation of motion for linear as well as nonlinear feedback cases. Let us rewrite our equation of motion as

$$\ddot{\phi} + \omega^2\phi = \mu_1\dot{\phi} + b_1\dot{\phi}^3 + \mu_2\phi^2\dot{\phi} + b_2\phi\dot{\phi}^2 + u \tag{2.59}$$

The additional term which we are adding here is u, the control feedback input, which was not used when we discussed open loop system.It is to be noted that u is scalar in this case.

Defining the state vector $\mathbf{x} = (x_1, x_2)^T = (\phi, \dot{\phi})^T$, the Eq. (2.59) can be written in the state variable form as

$$\dot{x_1} = x_2 \tag{2.60}$$

$$\dot{x_2} = -\omega^2 x_1 + \mu_1 x_2 + f(\mathbf{x}) + u \tag{2.61}$$

where

$$f(\mathbf{x}) = b_1 x_2^3 + \mu_2 x_1^2 x_2 + b_2 x_1 x_2^2 \tag{2.62}$$

If Eqs. (2.60) and (2.61) is written in the form as Eq. (2.40), then

$$\mathbf{A} = \begin{bmatrix} 0 & 1 \\ -\omega^2 & \mu_1 \end{bmatrix} \tag{2.63}$$

and

$$\mathbf{B} = \begin{bmatrix} 0 \\ 1 \end{bmatrix} \tag{2.64}$$

The method of finding optimal control for this nonlinear model starts by choosing the highest order term of $f(\mathbf{x})$ i.e., $2n-1=3$ or $n=2$. Therefore the performance index becomes

$$J = \frac{1}{2}\int_0^\infty \left\{ \begin{bmatrix} \mathbf{x} \\ \mathbf{x}^2 \end{bmatrix}^T \begin{bmatrix} \mathbf{Q}_{1,1} & \mathbf{Q}_{1,2} \\ \mathbf{Q}_{2,1} & \mathbf{Q}_{2,2} \end{bmatrix} \begin{bmatrix} \mathbf{x} \\ \mathbf{x}^2 \end{bmatrix} + u^2 \right\} dt \tag{2.65}$$

Note that R=1 here. Now the Lyapunov function is assumed to be

$$V(\mathbf{x}) = \frac{1}{2} \begin{bmatrix} \mathbf{x} \\ \mathbf{x}^2 \end{bmatrix}^T \begin{bmatrix} \mathbf{P}_{1,1} & \mathbf{P}_{1,2} \\ \mathbf{P}_{2,1} & \mathbf{P}_{2,2} \end{bmatrix} \begin{bmatrix} \mathbf{x} \\ \mathbf{x}^2 \end{bmatrix} \tag{2.66}$$

Setting

$$\mathbf{Q}_{1,1} = \begin{bmatrix} 1 & 0 \\ 0 & 1 \end{bmatrix} \tag{2.67}$$

and solving the algebraic Riccati equation, we get

$$\mathbf{P}_{1,1} = \begin{bmatrix} P_{1,1}(1,1) & P_{1,1}(1,2) \\ P_{1,1}(2,1) & P_{1,1}(2,2) \end{bmatrix} \tag{2.68}$$

where

$$P_{1,1}(1,1) = \omega^2\mu_1 + \frac{1}{2}(\omega^4+1)^{1/2}[4\mu_1^2 - 8\omega^2 + 8(\omega^4+1)^{1/2} + 4]^{1/2} \tag{2.69}$$

$$P_{1,1}(1,2) = P_{1,1}(2,1) = -\omega^2 + (\omega^4+1)^{1/2} \tag{2.70}$$

$$P_{1,1}(2,2) = \mu_1 + \frac{1}{2}[4\mu_1^2 - 8\omega^2 + 8(\omega^4+1)^{1/2} + 4]^{1/2} \tag{2.71}$$

Now

$$V_2(\mathbf{x}) = \frac{1}{2}\mathbf{x}^T\mathbf{P}_{1,1}\mathbf{x}$$

Therefore,

$$\left[\frac{\partial V_2(\mathbf{x})}{\partial \mathbf{x}}\right]^T = \mathbf{P_{1,1}x} = \begin{bmatrix} P_{1,1}(1,1)x_1 + P_{1,1}(1,2)x_2 \\ P_{1,1}(2,1)x_1 + P_{1,1}(2,2)x_2 \end{bmatrix} \tag{2.72}$$

and

$$V_3(\mathbf{x}) = \frac{1}{2}\mathbf{x}^T\mathbf{P_{1,2}}\mathbf{x}^2 + \frac{1}{2}(\mathbf{x}^2)^T\mathbf{P_{2,1}x}$$

Therefore

$$\left[\frac{\partial V_3(\mathbf{x})}{\partial \mathbf{x}}\right]^T = \begin{bmatrix} 3P_{2,1}(1,1)x_1^2 + 2P_{2,1}(2,1)x_1x_2 + P_{2,1}(1,2)x_2^2 \\ P_{2,1}(2,1)x_1^2 + 2P_{2,1}(1,2)x_1x_2 + 3P_{2,1}(2,2)x_2^2 \end{bmatrix} \tag{2.73}$$

Substituting Eqs. (2.72) and (2.73) into Eq. (2.55) and solving we get

$$\mathbf{P_{2,1}} = \mathbf{P_{1,2}} = \begin{bmatrix} P_{2,1}(1,1) & P_{2,1}(1,2) \\ P_{2,1}(2,1) & P_{2,1}(2,2) \end{bmatrix} \tag{2.74}$$

where

$$P_{2,1}(1,2) = P_{2,1}(2,1) = \frac{Q_{2,1}(1,1)}{[\omega^2 + P_{1,1}(1,2)]} \tag{2.75}$$

$$P_{2,1}(1,1) = \frac{1}{3}[-Q_{2,1}(1,2) + P_{1,1}(2,2)P_{2,1}(1,2) + 2P_{1,1}(1,2)P_{2,1}(1,2) + 2\omega^2 P_{2,1}(1,2) - \mu_1 P_{2,1}(1,2)] \tag{2.76}$$

$$P_{2,1}(2,2) = \frac{Q_{2,1}(1,2) - 2[P_{1,1}(2,2)P_{2,1}(1,2) - P_{2,1}(1,2) - \mu_1 P_{2,1}(1,2)]}{3\omega^2 + 3P_{1,1}(1,2)} \tag{2.77}$$

Since $n = 2$, we have

$$V_4(\mathbf{x}) = \frac{1}{2}(\mathbf{x}^2)^T\mathbf{P_{2,2}}\mathbf{x}^2$$

and

$$\left[\frac{\partial V_4(\mathbf{x})}{\partial \mathbf{x}}\right]^T = \begin{bmatrix} 2x_1^3P_{2,2}(1,1) + 2x_1x_2^2P_{2,2}(1,2) \\ 2x_2^3P_{2,2}(2,2) + 2x_2x_1^2P_{2,2}(1,2) \end{bmatrix} \tag{2.78}$$

substituting Eqs. (2.72), (2.73) and (2.78) into Eq. (2.57), we get

$$\mathbf{P_{2,2}} = \begin{bmatrix} P_{2,2}(1,1) & P_{2,2}(1,2) \\ P_{2,2}(1,2) & P_{2,2}(2,2) \end{bmatrix} \tag{2.79}$$

$$\mathbf{P_{2,2}(1,2)} = \mathbf{P_{2,2}(2,1)}$$

$$P_{2,2}(1,2) = \frac{2[P_{2,1}(1,2)]^2 + 3P_{2,1}(2,2)P_{2,1}(1,2) - Q_{2,2}(1,2) - b_2P_{1,1}(1,2) - \mu_2P_{1,1}(2,2)}{2\mu_1 - 2P_{1,1}(2,2)} \tag{2.80}$$

$$P_{2,2}(1,1) = [P_{2,1}(1,2)]^2 + \omega^2P_{2,2}(1,2) - 0.5\mu_2P_{1,1}(1,2) + P_{1,1}(1,2)P_{2,2}(1,2) \tag{2.81}$$

$$P_{2,2}(2,2) = -\frac{[6P_{2,1}(2,2)P_{2,1}(1,2) - 2P_{2,2}(1,2) - b_1P_{1,1}(1,2) - b_2P_{1,1}(2,2)]}{2[\omega^2 + P_{1,1}(1,2)]} \tag{2.82}$$

On substituting Eq. (2.72) into Eq. (2.49) we get the linear feedback optimal as

$$u(\mathbf{x}) = -[P_{1,1}(1,2)x_1 + P_{1,1}(2,2)x_2] \tag{2.83}$$

Similarly on substituting Eqs. (2.72), (2.73) and (2.78) into Eq. (2.49) we get the nonlinear feedback optimal control as

$$\begin{aligned} u(\mathbf{x}) &= -[P_{1,1}(1,2)x_1 + P_{1,1}(2,2)x_2 + 3x_2^2P_{2,1}(2,2) + (x_1^2 + 2x_1x_2)P_{2,1}(1,2) \\ &\quad +2x_2^3P_{2,2}(2,2) + 2x_2x_1^2P_{2,2}(1,2)] \end{aligned} \tag{2.84}$$

Furthur, these equations of $u(\mathbf{x})$ have been substituted in the equation of motion and Eqs. (2.60) and (2.61) have been solved with the help of Runge-Kutta method of $4^{th}/5^{th}$ order on MATLAB to obtain plots of roll angle and roll rate against time.

Feedback Using an Actuator for Control Surface

In the above case, we have assumed an imaginary actuator which is applying the feedback instantaneously as the output is obtained. In practical situation, such an assumption cannot be made. Therefore, in this part a modification in the above problem has been made by adding one more differential equation which will take care of the above discrepancy.

An aileron control surface with first order actuator dynamics is modeled as

$$\dot{\delta_A} = -\frac{1}{\tau}\delta_A + \frac{1}{\tau}\delta_{A_{COM}} \tag{2.85}$$

where δ_A is the aileron angle, $\delta_{A_{COM}}$ is the commanded aileron angle and τ is the time constant of the actuator. i.e., feedback time lag.

Now defining our state vector as $\mathbf{x} = (x_1, x_2, x_3)^T = (\phi, \dot{\phi}, \delta_A)^T$, our equation of motion can be written in the state variable form as

$$\dot{x_1} = x_2 \tag{2.86}$$

$$\dot{x_2} = -\omega^2 x_1 + \mu_1 x_2 + f(\mathbf{x}) + x_3 \tag{2.87}$$

$$\dot{x_3} = -k x_3 + k u \tag{2.88}$$

where $k = \frac{1}{\tau}$. If Eqs. (2.86), (2.87) and (2.88) are written in the form as Eq. (2.40), then

$$\mathbf{A} = \begin{bmatrix} 0 & 1 & 0 \\ -\omega^2 & \mu_1 & 1 \\ 0 & 0 & -k \end{bmatrix} \tag{2.89}$$

and

$$\mathbf{B} = \begin{bmatrix} 0 \\ 0 \\ k \end{bmatrix} \tag{2.90}$$

Setting

$$\mathbf{Q_{1,1}} = \begin{bmatrix} 1 & 0 & 0 \\ 0 & 1 & 0 \\ 0 & 0 & 1 \end{bmatrix} \tag{2.91}$$

and solving the algebraic Riccati equation we get

$$\mathbf{P_{1,1}} = \begin{bmatrix} P_{1,1}(1,1) & P_{1,1}(1,2) & P_{1,1}(1,3) \\ P_{1,1}(2,1) & P_{1,1}(2,2) & P_{1,1}(2,3) \\ P_{1,1}(3,1) & P_{1,1}(3,2) & P_{1,1}(3,3) \end{bmatrix} \tag{2.92}$$

As in the previous case, we can substitute the expression for $\partial V_2(\mathbf{x})/\partial \mathbf{x}$. $\partial V_3(\mathbf{x})/\partial \mathbf{x}$ and

$\partial V_4(\mathbf{x})/\partial \mathbf{x}$ in Eqs. (2.55) and (2.57) and solve these equations to obtain $\mathbf{P_{2,1}}$ and $\mathbf{P_{2,2}}$ where

$$\mathbf{P_{2,1}} = \mathbf{P_{1,2}} = \begin{bmatrix} P_{2,1}(1,1) & P_{2,1}(1,2) & P_{2,1}(1,3) \\ P_{2,1}(2,1) & P_{2,1}(2,2) & P_{2,1}(2,3) \\ P_{2,1}(3.1) & P_{2,1}(3,2) & P_{2,1}(3,3) \end{bmatrix} \tag{2.93}$$

and

$$\mathbf{P_{2,2}} = \begin{bmatrix} P_{2,2}(1,1) & P_{2,2}(1,2) & P_{2,2}(1,3) \\ P_{2,2}(2,1) & P_{2,2}(2,2) & P_{2,2}(2,3) \\ P_{2,2}(3,1) & P_{2,2}(3,2) & P_{2,2}(3,3) \end{bmatrix} \tag{2.94}$$

Although all the elements of the matrix $\mathbf{P_{2,1}}$ and $\mathbf{P_{2,2}}$ can be obtained by solving Eqs. (2.55) and (2.57), only those elements of $\mathbf{P_{2,1}}$ and $\mathbf{P_{2,2}}$ are given below which are required to solve our state variable equation.

$$P_{1,2}(1,3) = \frac{Q_{1,2}(1,3) + [Q_{1,2}(1,1)/\omega^2]}{2k^2P_{1,1}(3,1) + k^2P_{1,1}(3,3) + k + [k^2P_{1,1}(3,1)/\omega^2]} \tag{2.95}$$

$$P_{1,2}(1,2) = \frac{Q_{1,2}(1,1) - k^2P_{1,1}(1,3)P_{1,2}(1,3)}{\omega^2} \tag{2.96}$$

$$P_{1,2}(2,3) = \frac{P_{1,2}(1,3)[1 - k^2P_{1,1}(3,2)] + P_{1,2}(1,2)}{\omega^2 + k^2P_{1,1}(1,3)} \tag{2.97}$$

$$P_{1,2}(3,3) = \frac{Q_{1,2}(1,3) - 2k^2P_{1,1}(3,3)P_{1,2}(1,3) - \omega^2P_{1,2}(2,3) - 2kP_{1,2}(1,3)}{3k^2P_{1,1}(3,1)} \tag{2.98}$$

$$P_{2,2}(1,3) = -\frac{[P_{1,2}(1,3)]^2}{P_{1,1}(3,1)} \tag{2.99}$$

$$P_{2,2}(2,3) = \frac{b_2P_{1,1}(3,3) - 2k^2P_{1,2}(2,3)P_{1,2}(1,3)}{2k^2P_{1,1}(3,1)} \tag{2.100}$$

$$P_{2,2}(3,3) = -\frac{3P_{1,2}(1,3)P_{1,2}(3,3)}{P_{1,1}(3,1)} \tag{2.101}$$

The linear feedback optimal control for this case is

$$u(\mathbf{x}) = -k[P_{1,1}(1,3)x_1 + P_{1,1}(2,3)x_2 + P_{1,1}(3,3)x_3] \tag{2.102}$$

and the nonlinear feedback is

$$\begin{aligned} u(\mathbf{x}) \;=\; & -k[P_{1,1}(1,3)x_1 + P_{1,1}(2,3)x_2 + P_{1,1}(3,3)x_3 + P_{1,2}(1,3)x_1^2 + P_{1,2}(2,3)x_2^2 \\ & +2P_{1,2}(1,3)x_1x_3 + 2P_{1,2}(2,3)x_2x_3 + 3P_{1,2}(3,3)x_3^2 \\ & +2P_{2,2}(1,3)x_1^2x_3 + 2P_{2,2}(2,3)x_2^2x_3 + 2P_{2,2}(3,3)x_3^3] \end{aligned} \tag{2.103}$$

Substituting the values of $u(\mathbf{x})$ in Eq. (2.88) and solving Eqs. (2.86), (2.87) and (2.88) with the help of Runge-Kutta method of $4^{th}/5^{th}$ order on MATLAB, we obtain the plots of roll angle, roll rate and aileron angle against time.

Feedback Considering Sideslip Effects

Until now, we have not considered the effects of sideslip on the motion of aircraft. In this section we will see the variation of sideslip angle and sideslip rate with time and their overall effect on other parameters.

We define our state variable vector as $\mathbf{x} = (x_1, x_2, x_3, x_4, x_5)^T = (\phi, \dot{\phi}, \delta_A, \beta, \dot{\beta})^T$. Our equation of motion can be written as

$$\dot{x_1} = x_2 \tag{2.104}$$

$$\dot{x_2} = -\omega^2 x_1 + \mu_1 x_2 + L_\beta x_4 - L_r x_5 + f(x) + x_3 \tag{2.105}$$

$$\dot{x_3} = -k x_3 + k u \tag{2.106}$$

$$\dot{x_4} = x_5 \tag{2.107}$$

$$\dot{x_5} = -N_\beta x_4 + N_r x_5 - N_p x_2 \tag{2.108}$$

where, L_β is the dihedral effect, L_r is the roll moment due to yaw rate, N_β is the directional stability, N_r is the yaw rate damping and N_p is the yaw moment due to roll rate.

For this case the corresponding **A** and **B** matrices are

$$\mathbf{A} = \begin{bmatrix} 0 & 1 & 0 & 0 & 0 \\ -\omega^2 & \mu_1 & 1 & L_\beta & -L_r \\ 0 & 0 & -k & 0 & 0 \\ 0 & 0 & 0 & 0 & 1 \\ 0 & N_p & 0 & -N_\beta & N_r \end{bmatrix} \tag{2.109}$$

$$\mathbf{B} = \begin{bmatrix} 0 \\ 0 \\ k \\ 0 \\ 0 \end{bmatrix} \tag{2.110}$$

Setting

$$\mathbf{Q_{1,1}} = \begin{bmatrix} 1 & 0 & 0 & 0 & 0 \\ 0 & 1 & 0 & 0 & 0 \\ 0 & 0 & 1 & 0 & 0 \\ 0 & 0 & 0 & 1 & 0 \\ 0 & 0 & 0 & 0 & 1 \end{bmatrix} \tag{2.111}$$

Using these values of $\mathbf{A}$, $\mathbf{B}$ and $\mathbf{Q_{1,1}}$ and solving the algebraic Riccati equation we get $\mathbf{P_{1,1}}$ where

$$\mathbf{P_{1,1}} = \begin{bmatrix} P_{1,1}(1,1) & P_{1,1}(1,2) & P_{1,1}(1,3) & P_{1,1}(1,4) & P_{1,1}(1,5) \\ P_{1,1}(2,1) & P_{1,1}(2,2) & P_{1,1}(2,3) & P_{1,1}(2,4) & P_{1,1}(2,5) \\ P_{1,1}(3,1) & P_{1,1}(3,2) & P_{1,1}(3,3) & P_{1,1}(3,4) & P_{1,1}(3,5) \\ P_{1,1}(4,1) & P_{1,1}(4,2) & P_{1,1}(4,3) & P_{1,1}(4,4) & P_{1,1}(4,5) \\ P_{1,1}(5,1) & P_{1,1}(5,2) & P_{1,1}(5,3) & P_{1,1}(5,4) & P_{1,1}(5,5) \end{bmatrix} \tag{2.112}$$

Now solving the Eqs. (2.55) and (2.57) after substituting the expressions of $\partial V_2(\mathbf{x})/\partial \mathbf{x}$, $\partial V_3(\mathbf{x})/\partial \mathbf{x}$ and $\partial V_4(\mathbf{x})/\partial \mathbf{x}$ in them we get $\mathbf{P_{2,1}}$ and $\mathbf{P_{2,2}}$ where

$$\mathbf{P_{2,1}} = \mathbf{P_{1,2}} = \begin{bmatrix} P_{2,1}(1,1) & P_{2,1}(1,2) & P_{2,1}(1,3) & P_{2,1}(1,4) & P_{2,1}(1,5) \\ P_{2,1}(2,1) & P_{2,1}(2,2) & P_{2,1}(2,3) & P_{2,1}(2,4) & P_{2,1}(2,5) \\ P_{2,1}(3,1) & P_{2,1}(3,2) & P_{2,1}(3,3) & P_{2,1}(3,4) & P_{2,1}(3,5) \\ P_{2,1}(4,1) & P_{2,1}(4,2) & P_{2,1}(4,3) & P_{2,1}(4,4) & P_{2,1}(4,5) \\ P_{2,1}(5,1) & P_{2,1}(5,2) & P_{2,1}(5,3) & P_{2,1}(5,4) & P_{2,1}(5,5) \end{bmatrix} \tag{2.113}$$

and

$$\mathbf{P_{2,2}} = \begin{bmatrix} P_{2,2}(1,1) & P_{2,2}(1,2) & P_{2,2}(1,3) & P_{2,2}(1,4) & P_{2,2}(1,5) \\ P_{2,2}(2,1) & P_{2,2}(2,2) & P_{2,2}(2,3) & P_{2,2}(2,4) & P_{2,2}(2,5) \\ P_{2,2}(3,1) & P_{2,2}(3,2) & P_{2,2}(3,3) & P_{2,2}(3,4) & P_{2,2}(3,5) \\ P_{2,2}(4,1) & P_{2,2}(4,2) & P_{2,2}(4,3) & P_{2,2}(4,4) & P_{2,2}(4,5) \\ P_{2,2}(5,1) & P_{2,2}(5,2) & P_{2,2}(5,3) & P_{2,2}(5,4) & P_{2,2}(5,5) \end{bmatrix} \tag{2.114}$$

Those values of matrices $\mathbf{P_{2,1}}$ and $\mathbf{P_{2,2}}$ are given below which required to solve our equation of motion.

$$P_{1,2}(3,1) = \frac{\omega^2 Q_{1,2}(1,3) + Q_{1,2}(1,1)}{\omega^2[2k^2 P_{1,1}(3,1) + 2k^2 P_{1,1}(3,3) + k] + k^2 P_{1,1}(3,1)} \tag{2.115}$$

$$P_{1,2}(3,4) = -\frac{P_{1,1}(3,4)P_{1,2}(3,1)}{P_{1,1}(3,1)} \tag{2.116}$$

$$P_{1,2}(3,5) = \frac{P_{1,1}(3,5)P_{1,2}(3,4)}{P_{1,1}(3,4)} \tag{2.117}$$

$$P_{1,2}(2,1) = \frac{Q_{1,2}(1,1) - k^2 P_{1,1}(3,1)P_{1,2}(3,1)}{\omega^2} \tag{2.118}$$

$$P_{1,2}(3,2) = \frac{[2 - 2k^2 P_{1,1}(3,2)]P_{1,2}(3,1) + 2P_{1,2}(2,1)}{2k^2 P_{1,1}(3,1) + 2\omega^2} \tag{2.119}$$

$$P_{1,2}(3,3) = \frac{Q_{1,2}(3,1) - 2P_{1,2}(3,1)[k^2 P_{1,1}(3,3) + k] - \omega^2 P_{1,2}(3,2)}{3k^2 P_{1,1}(3,1)} \tag{2.120}$$

$$P_{2,2}(3,1) = -\frac{[P_{1,2}(3,1)]^2}{P_{1,1}(3,1)} \tag{2.121}$$

$$P_{2,2}(3,2) = \frac{b_2 P_{1,1}(3,3) - 2k^2 P_{1,2}(3,2)P_{1,2}(3,1)}{2k^2 P_{1,1}(3,1)} \tag{2.122}$$

$$P_{2,2}(3,3) = -\frac{3P_{1,2}(3,1)P_{1,2}(3,3)}{P_{1,1}(3,1)} \tag{2.123}$$

$$P_{2,2}(3,4) = -\frac{P_{1,2}(3,1)P_{1,2}(3,4)}{P_{1,1}(3,1)} \tag{2.124}$$

$$P_{2,2}(3,5) = -\frac{P_{1,2}(3,1)P_{1,2}(3,5)}{P_{1,1}(3,1)} \tag{2.125}$$

The linear feedback in this case is

$$u(\mathbf{x}) = -k[P_{1,1}(3,1)x_1 + P_{1,1}(3,2)x_2 + P_{1,1}(3,3)x_3 + P_{1,1}(3,4)x_4 + P_{1,1}(3,5)x_5] \tag{2.126}$$

and the nonlinear feedback is

$$\begin{aligned} u(\mathbf{x}) \;=\; & -k[P_{1,1}(3,1)x_1 + P_{1,1}(3,2)x_2 + P_{1,1}(3,3)x_3 + P_{1,1}(3,4)x_4 + P_{1,1}(3,5)x_5 \\ & + P_{1,2}(3,1)x_1^2 + P_{1,2}(3,2)x_2^2 + 2P_{1,2}(3,1)x_1x_3 + 2P_{1,2}(3,2)x_2x_3 + 3P_{1,2}(3,3)x_3^2 \\ & + 2P_{1,2}(3,4)x_3x_4 + 2P_{1,2}(3,5)x_3x_5 + P_{1,2}(3,4)x_4^2 + P_{1,2}(3,5)x_5^2 + 2P_{2,2}(3,1)x_1^2x_3 \\ & + 2P_{2,2}(3,2)x_2^2x_3 + 2P_{2,2}(3,3)x_3^3 + 2P_{2,2}(3,4)x_3x_4^2 + 2P_{2,2}(3,5)x_3x_5^2] \end{aligned} \tag{2.127}$$

Finally these values of $u(\mathbf{x})$ are substituted in the state variable equations and solved with the help of Runge-Kutta method of $4^{th}/5^{th}$ order on MATLAB to obtain plots of roll angle, roll rate, aileron angle, sideslip angle and sideslip rate against time.

Chapter 3

NUMERICAL RESULTS

For the demonstration of the methodology discussed in the previous Chapter, same delta wing, which has been used in Refs. [2] and [8], is taken here. The particulars of the delta wing is given below.

Leading-edge-sweep angle = 80 deg

Aspect ratio = 0.705

Chord = 0.429m

L_c = Chord/4

Area = $0.0324m^2$

Mass = 0.284kg

$I_x = 0.27 \times 10^{-3}$kg-$m^2$

$\rho_{air} = 0.12 \times 10^{-2}$kg/$m^3$

U_c = 15m/s

$\mu_x = 0.378 \times 10^{-4}$kg-$m^4$

This value of μ_x was found by trial and error to be the only value for which onset angle, period and amplitude agree with the experiment. These choices lead to $C_1 = 0.354$ and $C_2 = 0.001$.

3.1 Response of Open Loop System

To know about the character of motion at non-equilibrium positions, we solve Eqs. (2.28) and (2.29) using Runge-Kutta method of $4^{th}/5^{th}$ order on MATLAB. The plots which have been obtained, of roll angle and roll rate with respect to time, indicates the wing rock motion to be a limit cycle motion.

The amplitude of the limit cycle motion depends on the angle of attack as it can be observed from Fig. (3.1). An early transition to limit cycle motion along with increased amplitude is observed, as the angle of attack increases. The corresponding phase plane plots for second order system of roll angle and roll rate for three angles of attack is shown in Fig. (3.2). Fig. (3.3) shows the wing rock motion triggered by roll angle for fifth order system at $\alpha = 25$ deg. Fig. (3.3a) and Fig. (3.3b) exhibit limit cycle motion for roll angle and roll rate respectively whereas Fig. (3.3c) and Fig. (3.3d) exhibit limit cycle limit cycle motion for sideslip angle and sideslip rate respectively. It can be observed from Fig. (3.3d) that initially sideslip rate increases sharply and then transits into limit cycle motion. Fig. (3.3e) shows the corresponding phase plane plot of roll angle and roll rate whereas, Fig. (3.3f) shows the phase plane plot of sideslip angle and sideslip rate.

It has been stated earlier that limit cycle motion may be initiated by sideslip as well. In fact, this behaviour has been observed, even for very small sideslip angle of 0.01 rad. Fig. (3.4) shows the wing rock motion triggered by sideslip angle for fifth order system at $\alpha = 25$ deg. Fig. (3.4a) and Fig. (3.4b) show the roll angle and roll rate, starting from zero, attain limit cycle motion in 1200 sec. Fig. (3.4c) shows that the sideslip angle, starting from 0.01 rad, after initial fluctuations attains limit cycle motion. Similar behaviour has been observed from Fig. (3.4d) for sideslip rate, but in this case its initial value is 0 rad/s. Fig. (3.4e) shows the corresponding phase plane plot of roll angle and roll rate and Fig. (3.4e) and Fig. (3.4f) shows the corresponding phase plane plot of sideslip angle and sideslip rate. This exhibition of wing rock by sideslip is due to the small dihedral effect which has been considered in our model.

3.2 Response of Closed Loop System

For the second order state variable, we observe that our model gets stabilized in approximately 6 secs. for small initial conditions of $(\phi, \dot{\phi})$=(0.35 rad, 0 rad/s) for both nonlinear and linear feedback cases. In fact, no appreciable difference has been observed between nonlinear and linear feedback responses for these initial conditions as it can be observed from Fig. (3.5). Fig. (3.5a) shows nonlinear feedback response at $\alpha = 25$ deg whereas Fig. (3.5b) shows linear feedback response at $\alpha = 25$ deg. Fig. (3.5c) shows the corresponding phase plane plot of roll angle and roll rate of nonlinear and linear feedback response. In Fig. (3.3a) and Fig. (3.3c) the results obtained are compared with the results obtained in Ref. (14). As it can be observed from these plots that the results obtained in this thesis is same as what it has been obtained in Ref. (14). Also it has been observed for nonlinear as well as linear cases that for these small initial conditions feedback responses at different angles of attack are found to be same. Whereas for large initial conditions of $(\phi, \dot{\phi})$=(1.4 rad, 3.5 rad/s), nonlinear feedback response proves to be better than linear feedback response, as it can be observed from Fig. (3.6). For $\alpha = 25$ deg, linear feedback response even gets diverged in 0.37 seconds. But in case of wing rock, the amplitudes of limit cycle motion for our model at $\alpha = 25$ deg are $(\phi, \dot{\phi})$=(0.6 rad, 0.08 rad/s). Thus at these initial conditions, it has been observed that both nonlinear as well as linear feedback responses are found to be equally effective in supressing wing rock motion. Here it has been assumed that $Q_{1,2}(1,1) = 1/64$, $Q_{1,2}(1,2) = 0$ and $Q_{2,2}(1,2) = 0$.

For the third order state variable, similar features like second order have been observed. But in this case, for initial conditions of $(\phi, \dot{\phi}, \delta_A)$ =(0.35 rad, 0 rad/s, 0 rad), the time to stabilize has increased to 8 secs., as it can be observed from Fig. (3.7a) and Fig. (3.7b). This expected increase in time is due to the use of actuator with time constant $\tau = 0.0495$ s. The maximum aileron deflection has been observed to be -0.21 rad for both nonlinear as well as linear feedback response. Fig. (3.7c) shows the corresponding phase plane plot of roll angle and roll rate. When the initial conditions are $(\phi, \dot{\phi}, \delta_A)$=(0.6 rad. 0.08 rad/s. 0 rad). the stabilization time remains

almost same, but the maximum aileron deflection has increased to -0.45 rad. as it can be observed from Fig. (3.8a). Fig. (3.8b) shows the phase plane plot for nonlinear and linear feedback response at $\alpha = 25$ deg. and Fig. (3.8c) shows the comparison phase plane plot of nonlinear feedback response at different angles of attack. It has been assumed that $Q_{1,2}(1,1) = 1/64$ and $Q_{1,2}(1,3) = 0$. The $P_{1,1}$ matrix, which has been obtained by solving the algebraic Riccati equation for three angles of attack are given below.

$$\mathbf{P}_{1,1_{\alpha=25deg}} = \begin{bmatrix} 1.97 & 1.4404 & 0.048 \\ 1.4404 & 2.8934 & 0.098275 \\ 0.048 & 0.098275 & 0.02386 \end{bmatrix}$$

$$\mathbf{P}_{1,1_{\alpha=22.5deg}} = \begin{bmatrix} 1.9734 & 1.4476 & 0.0483 \\ 1.4476 & 2.8889 & 0.0981 \\ 0.0483 & 0.0981 & 0.0239 \end{bmatrix}$$

$$\mathbf{P}_{1,1_{\alpha=21.5deg}} = \begin{bmatrix} 1.9751 & 1.451 & 0.0484 \\ 1.451 & 2.8875 & 0.0981 \\ 0.0484 & 0.0981 & 0.0239 \end{bmatrix}$$

For the fifth order state variable, where we have also considered beta dynamics, the nonlinear and linear feedback responses for the initial conditions $(\phi, \dot{\phi}, \delta_A, \beta, \dot{\beta})$=(0.35 rad, 0 rad/s, 0 rad, 0rad, 0 rad/s) is found to be almost overlapping on each other. But for the clarity, only nonlinear feedback response is shown in Fig. (3.9). In Fig. (3.9a) responses of all the five state variables have been shown with respect to time. Fig. (3.9b) shows the corresponding phase plane plot of roll angle and roll rate at different angles of attack and Fig. (3.9c) shows the corresponding phase plane plot of sideslip angle and sideslip rate at different angles of attack. Fig. (3.10) shows the nonlinear and linear feedback response for the initial conditions $(\phi, \dot{\phi}, \delta_A, \beta, \dot{\beta})$=(0.6 rad, 0.08 rad/s, 0 rad, 0 rad, 0 rad/s). In this case the roll angle, roll rate and aileron angle stabilize in almost 8 sec, but the sideslip angle and the sideslip rate continue to fluctuate till 45 sec. Fig. (3.11) shows the corresponding phase plane plots. Fig.

(3.11a) shows the phase plane plot of roll angle and roll rate for nonlinear and linear feedback response at $\alpha = 25$ deg. whereas Fig. (3.11b) shows the corresponding phase plane plot for sideslip angle and sideslip rate. A comparison phase plane plot for nonlinear feedback response at different angles of attack for roll angle and roll rate and sideslip angle and sideslip rate has been shown in Fig. (3.11c) and Fig. (3.11d) respectively. Very little variation in these phase plane plots have been observed as the angle of attack varies. It has been assumed that the magnitude of $L_\beta = -0.02822$, $L_r = 0.1517$, $N_\beta = 1.3214$, $N_r = -0.2491$ and $N_p = -0.0629$, for all the three angles of attack considered in this thesis, because of their negligible variation for these three angles of attack. In this case also $Q_{1,2}(1,1) = 1/64$ and $Q_{1,2}(1,3) = 0$ has been assumed. The $P_{1,1}$ matrix for three angles of attack are given below.

$$\mathbf{P_{1,1}}_{\alpha=25deg} = \begin{bmatrix} 1.9726 & 1.4408 & 0.048 & -0.0726 & -0.1504 \\ 1.4408 & 2.9118 & 0.0989 & 0.2209 & -0.372 \\ 0.048 & 0.0989 & 0.0239 & 0.0078 & -0.0126 \\ -0.0726 & 0.2209 & 0.0078 & 4.7865 & 0.3642 \\ -0.1504 & -0.372 & -0.0126 & 0.3642 & 3.5666 \end{bmatrix}$$

$$\mathbf{P_{1,1}}_{\alpha=22.5deg} = \begin{bmatrix} 1.9759 & 1.448 & 0.0483 & -0.0709 & -0.1506 \\ 1.448 & 2.9067 & 0.0987 & 0.221 & -0.3711 \\ 0.0483 & 0.0987 & 0.0239 & 0.0078 & -0.0125 \\ -0.0709 & 0.221 & 0.0078 & 4.7867 & 0.3642 \\ -0.1506 & -0.3711 & -0.0125 & 0.3642 & 3.5667 \end{bmatrix}$$

$$\mathbf{P_{1,1}}_{\alpha=21.5deg} = \begin{bmatrix} 1.9776 & 1.4514 & 0.0484 & -0.0702 & -0.1507 \\ 1.4514 & 2.9053 & 0.0987 & 0.2210 & -0.3707 \\ 0.0484 & 0.0987 & 0.0239 & 0.0078 & -0.0125 \\ -0.0702 & 0.221 & 0.0078 & 4.7867 & 0.3742 \\ -0.1507 & -0.3707 & -0.0125 & 0.3642 & 3.5667 \end{bmatrix}$$

A comparison between second, third and fifth order state variable has been shown in Fig. (3.12). From this figure, it can be observed that the stabilization time for

the third and fifth order state variable remains approximately same. This is due to the fact that same actuator has been used for the two cases and the dihedral effect considered here is quite small. If dihedral effect is large, then appreciable difference between the third order and the fifth order state variable will be observed, even if same actuator is used for both the cases.

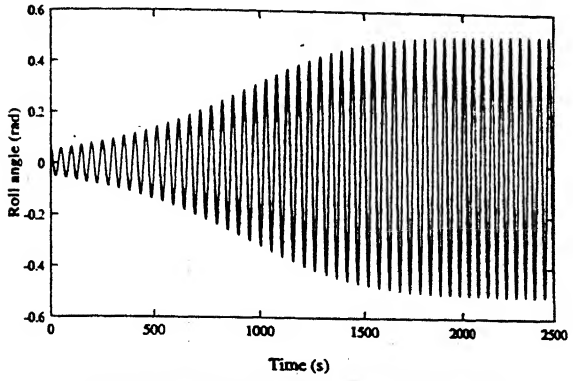

Fig.(3.1a) Limit cycle motion of Roll angle at alpha=21.5 deg.

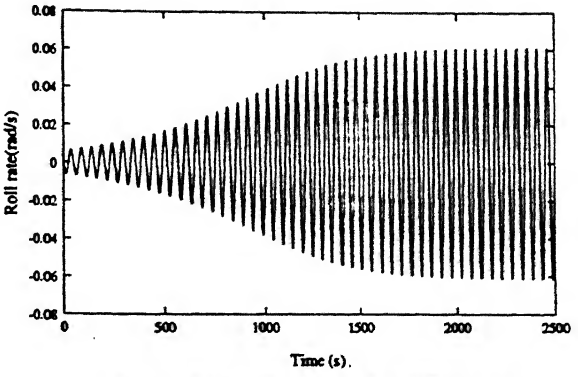

Fig.(3.1b) Limit cycle motion of Roll rate at alpha=21.5 deg.

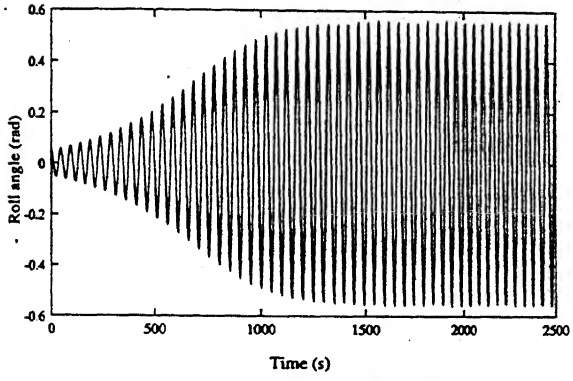

Fig.(3.1c) Limit cycle motion of Roll angle at alpha=22.5 deg.

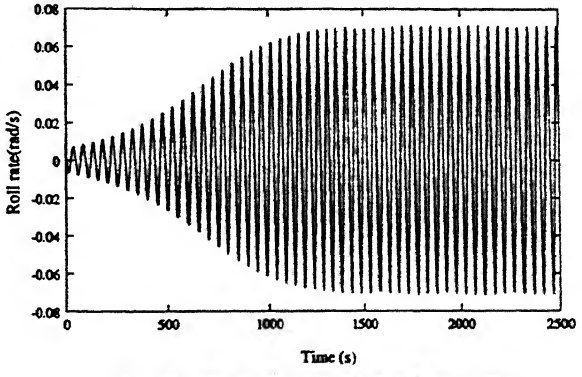

Fig.(3.1d) Limit cycle motion of Roll rate at alpha=22.5 deg.

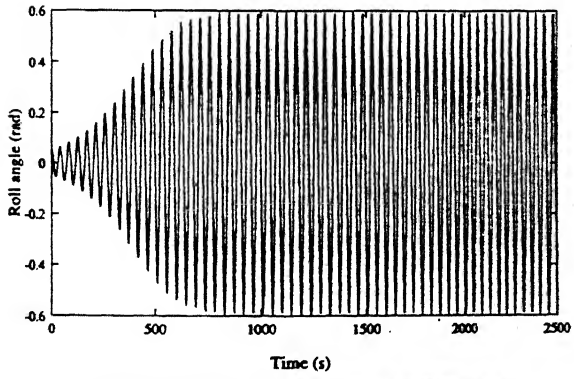

Fig.(3.1e) Limit cycle motion of Roll angle at alpha=25 deg.

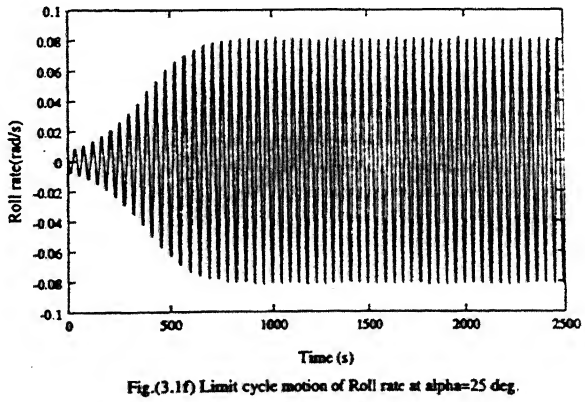

Fig.(3.1f) Limit cycle motion of Roll rate at alpha=25 deg.

Figure 3.1: Comparison of limit cycle motion triggered by roll angle at different angles of attack for second order state variable.

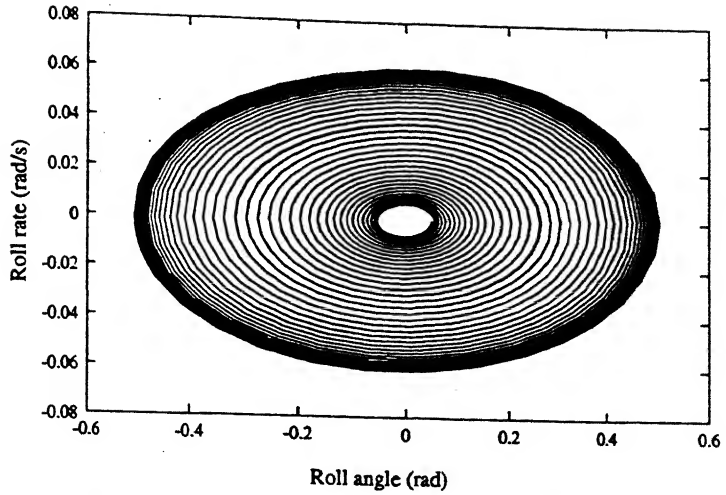

Fig.(3.2a) Phase plane plot for open loop system at alpha=21.5 deg.

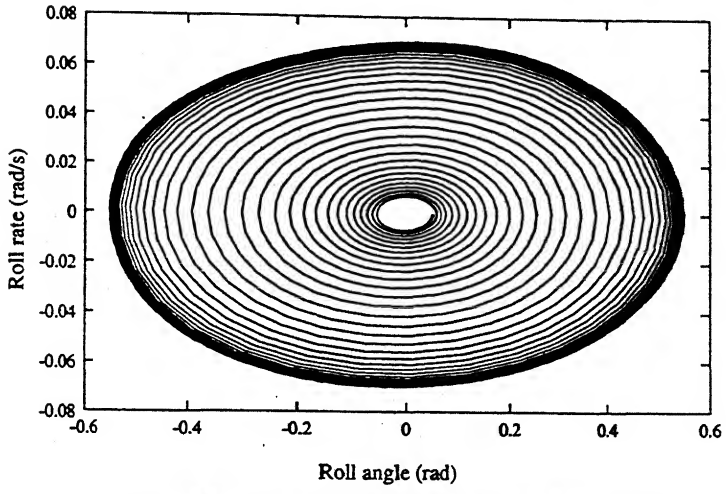

Fig.(3.2b) Phase plane plot for open loop systemat alpha=22.5 deg.

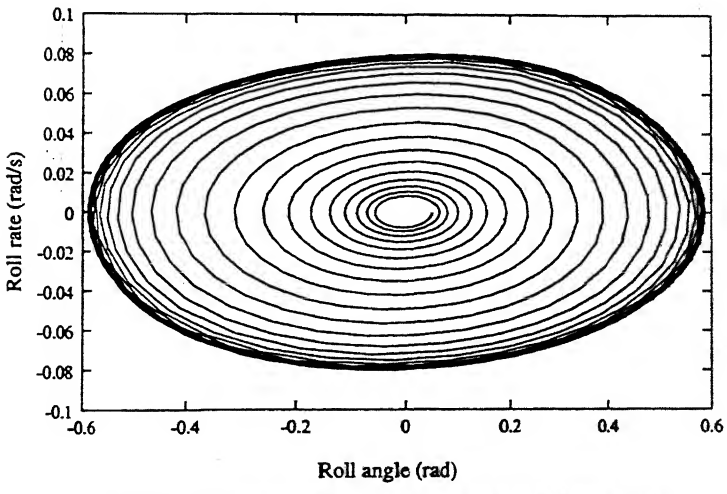

Fig.(3.2c) Phase plane plot for open loop system at alpha=25 deg.

Figure 3.2: Comparison of phase plane plots at different angles of attack for second order state variable.

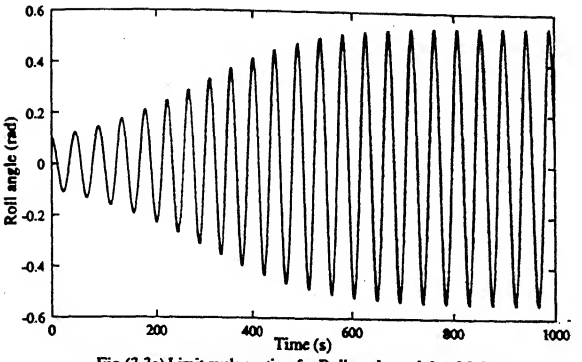

Fig.(3.3a) Limit cycle motion for Roll angle at alpha=25 deg.

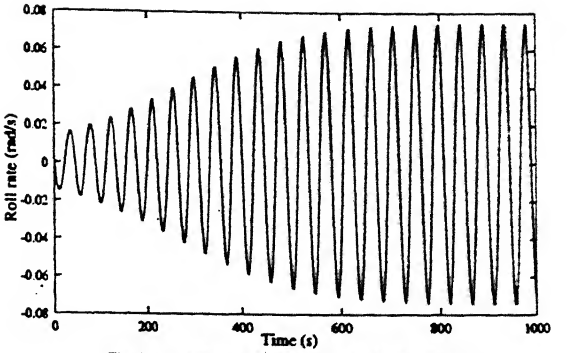

Fig.(3.3b) Limit cycle motion for Roll rate at alpha=25 deg.

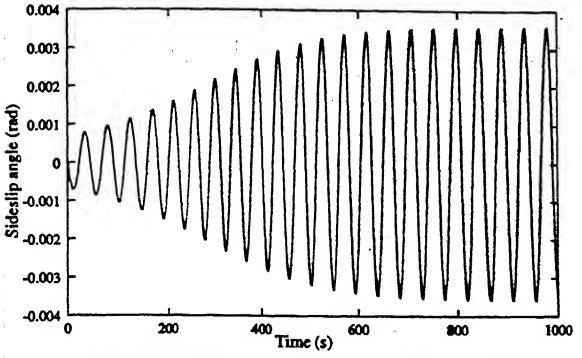

Fig.(3.3c) Limit cycle motion for Sideslip angle at alpha=25 deg.

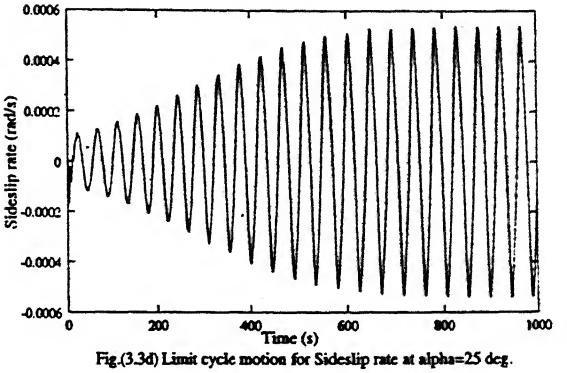

Fig.(3.3d) Limit cycle motion for Sideslip rate at alpha=25 deg.

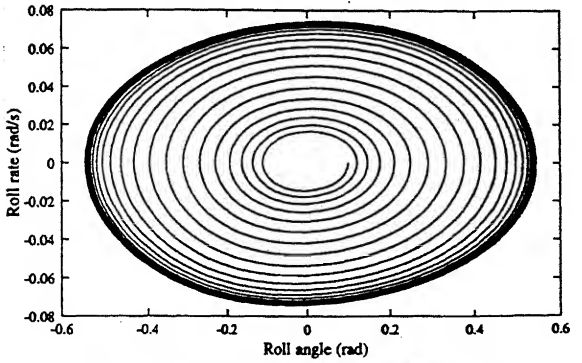

Fig.(3.3e) Phase plane plot for open loop system at alpha=25 deg.

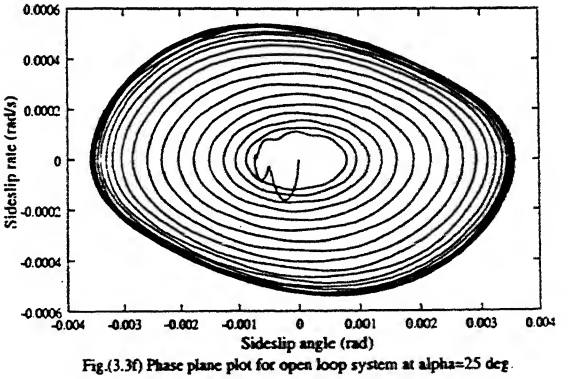

Fig.(3.3f) Phase plane plot for open loop system at alpha=25 deg.

Figure 3.3: Wing Rock motion triggered by roll angle for fifth order state variable at $\alpha = 25$ deg.

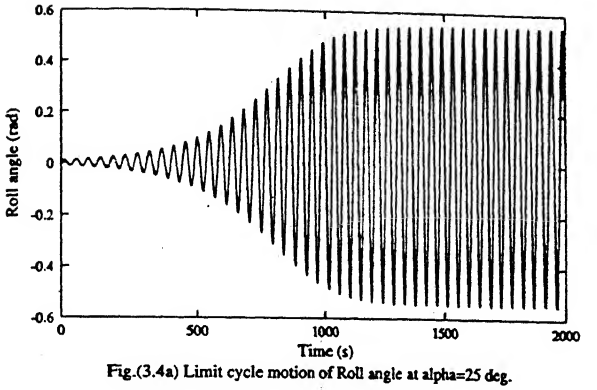

Fig.(3.4a) Limit cycle motion of Roll angle at alpha=25 deg.

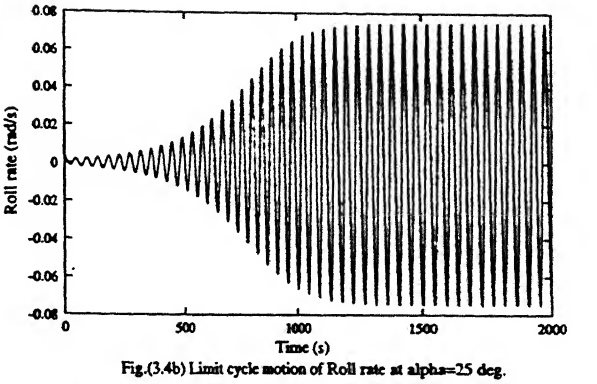

Fig.(3.4b) Limit cycle motion of Roll rate at alpha=25 deg.

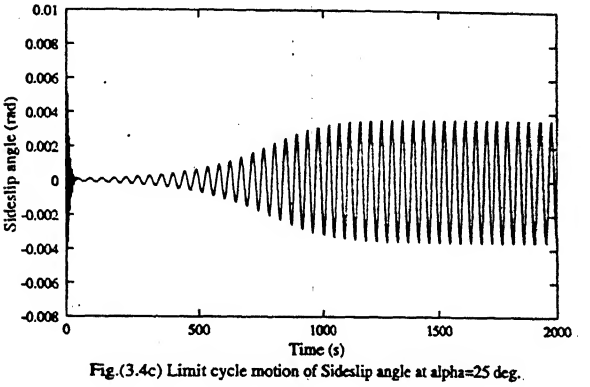

Fig.(3.4c) Limit cycle motion of Sideslip angle at alpha=25 deg.

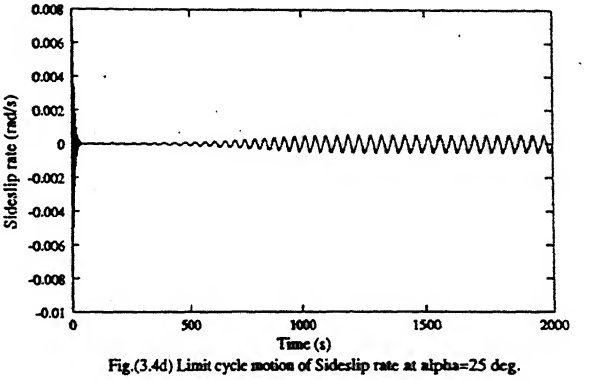

Fig.(3.4d) Limit cycle motion of Sideslip rate at alpha=25 deg.

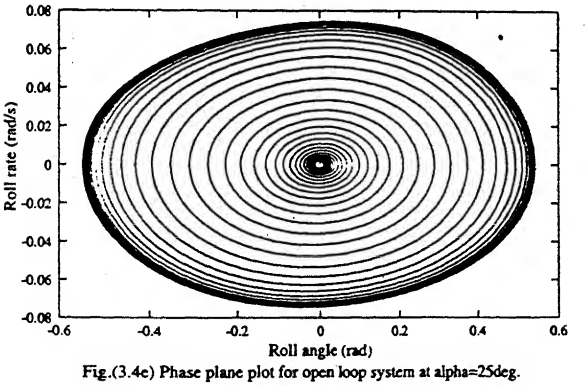

Fig.(3.4e) Phase plane plot for open loop system at alpha=25deg.

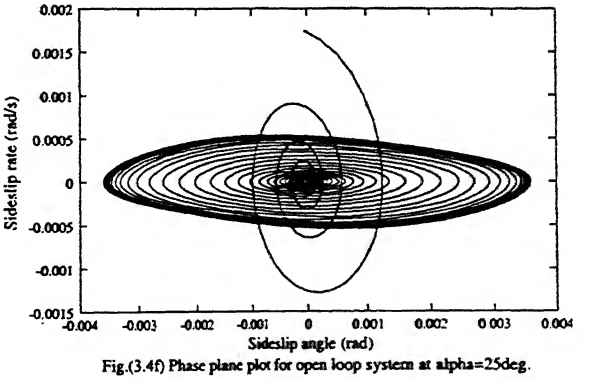

Fig.(3.4f) Phase plane plot for open loop system at alpha=25deg.

Figure 3.4: Wing Rock motion triggered by sideslip angle for fifth order state variable at $\alpha = 25$ deg.

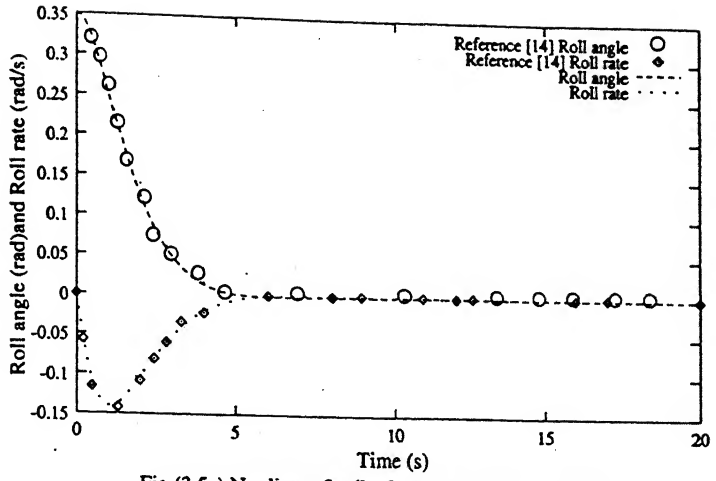

Fig.(3.5a) Nonlinear feedback response at alpha=25 deg.

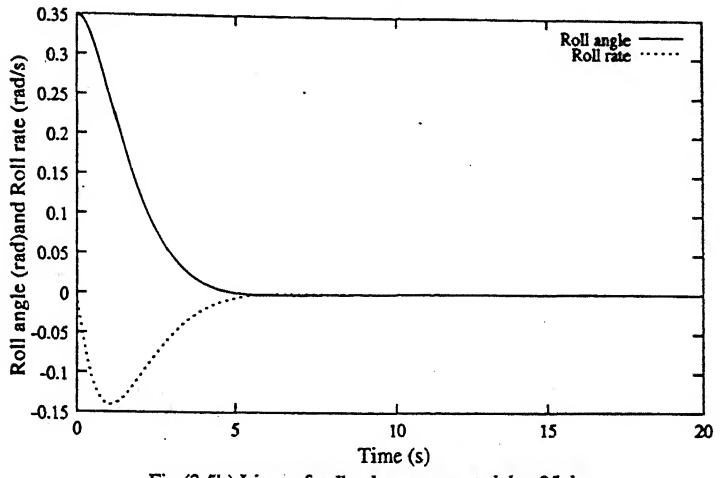

Fig.(3.5b) Linear feedback response at alpha=25 deg.

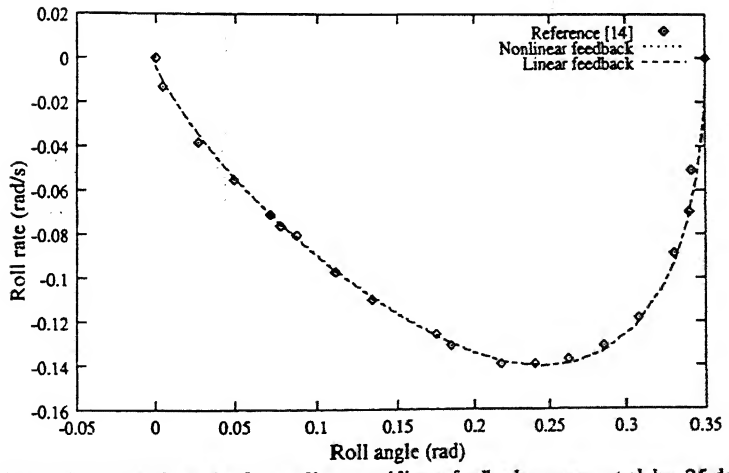

Fig.(3.5c) Phase plane plot for nonlinear and linear feedback response at alpha=25 deg.

Figure 3.5: Nonlinear and linear feedback response for second order state variable at $\alpha = 25$ deg, with initial conditions $(\phi, \dot{\phi})$=(0.35 rad, 0 rad/s).

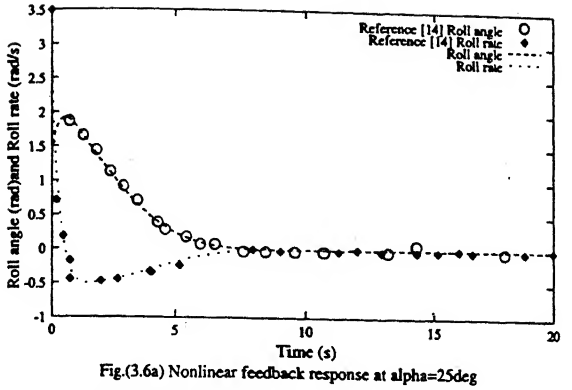

Fig.(3.6a) Nonlinear feedback response at alpha=25deg

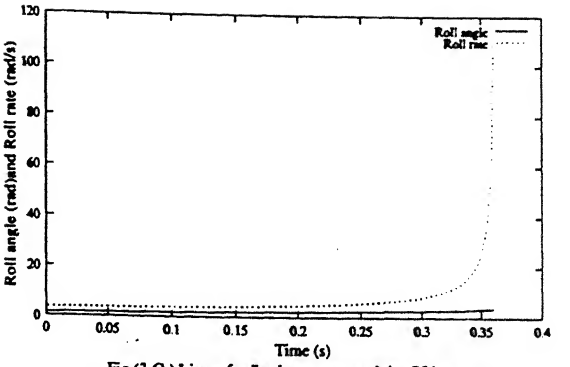

Fig.(3.6b) Linear feedback response at alpha=25deg

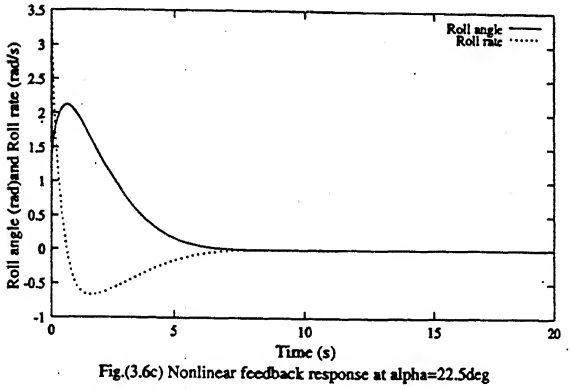

Fig.(3.6c) Nonlinear feedback response at alpha=22.5deg

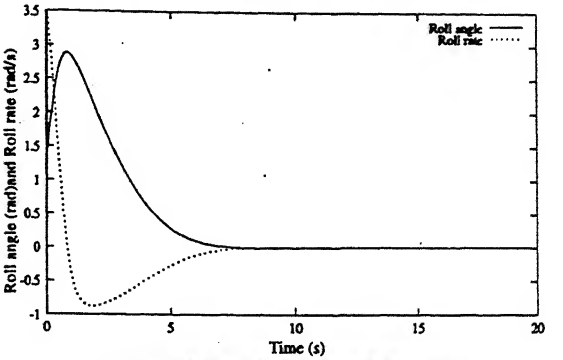

Fig.(3.6d) Linear feedback response at alpha=22.5deg

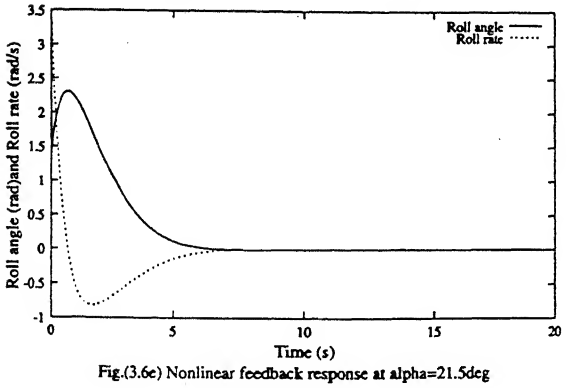

Fig.(3.6e) Nonlinear feedback response at alpha=21.5deg

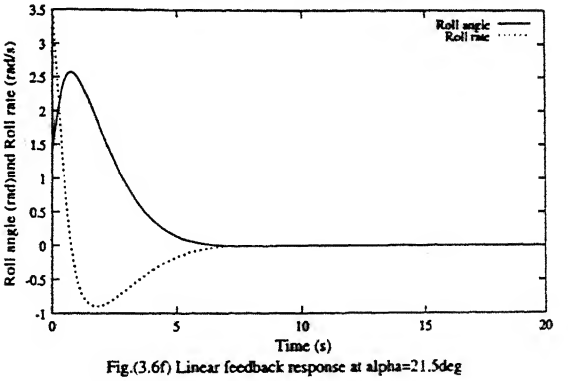

Fig.(3.6f) Linear feedback response at alpha=21.5deg

Figure 3.6: Comparison of nonlinear and linear feedback response for second order state variable at different angles of attack, with initial conditions $(\phi, \dot{\phi})$=(1.4 rad, 3.5 rad/s).

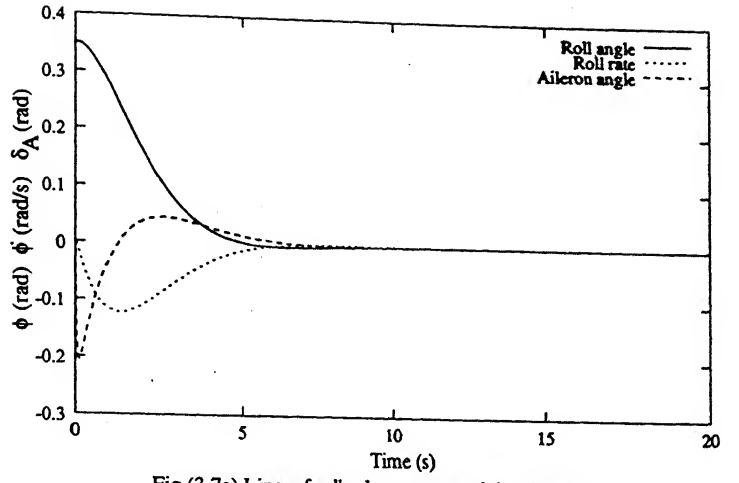

Fig.(3.7a) Linear feedback response at alpha=25deg

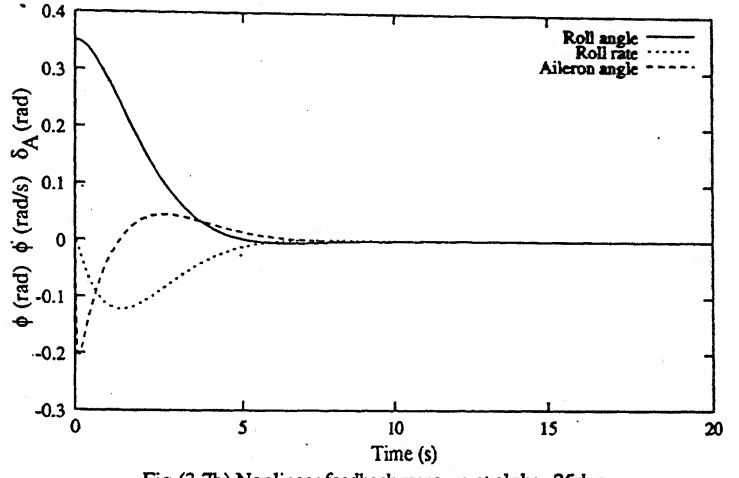

Fig.(3.7b) Nonlinear feedback response at alpha=25deg.

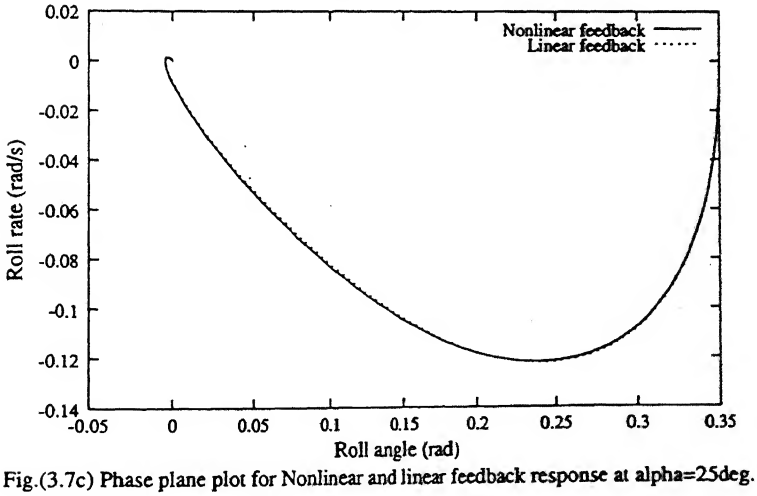

Fig.(3.7c) Phase plane plot for Nonlinear and linear feedback response at alpha=25deg.

Figure 3.7: Nonlinear and linear feedback response at $\alpha = 25$ deg for third order state variable with initial conditions $(\phi, \dot{\phi}, \delta_A)$=(0.35 rad, 0 rad/s, 0 rad).

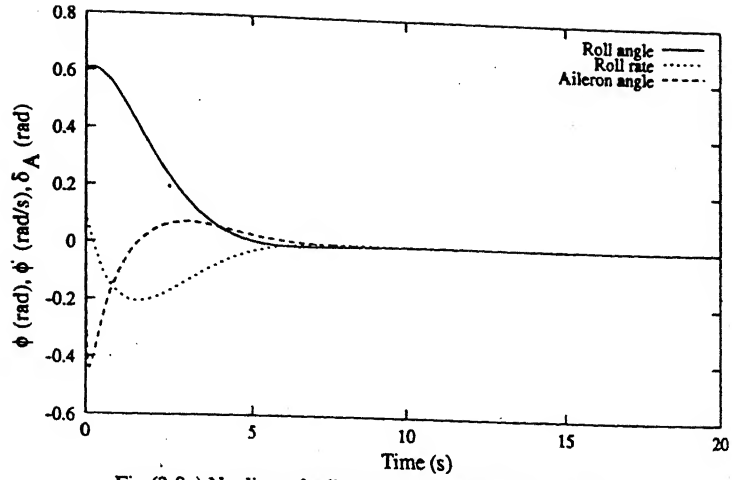

Fig.(3.8a) Nonlinear feedback response at alpha=25 deg.

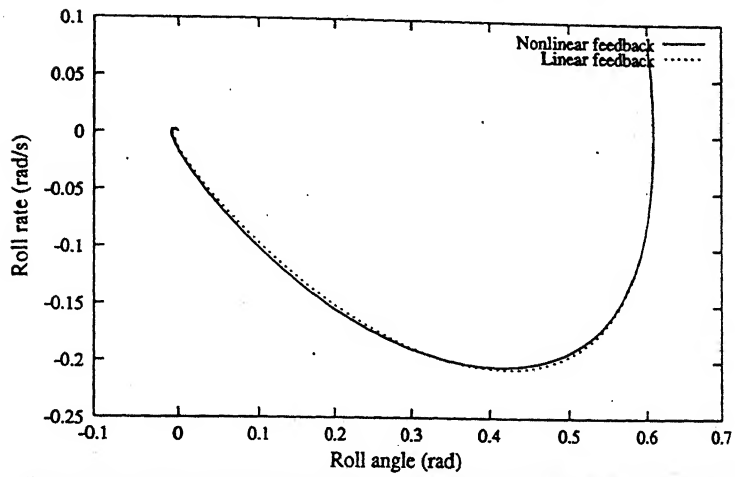

Fig.(3.8b) Phase plane plot of nonlinear and linear feedback response at alpha=25 deg.

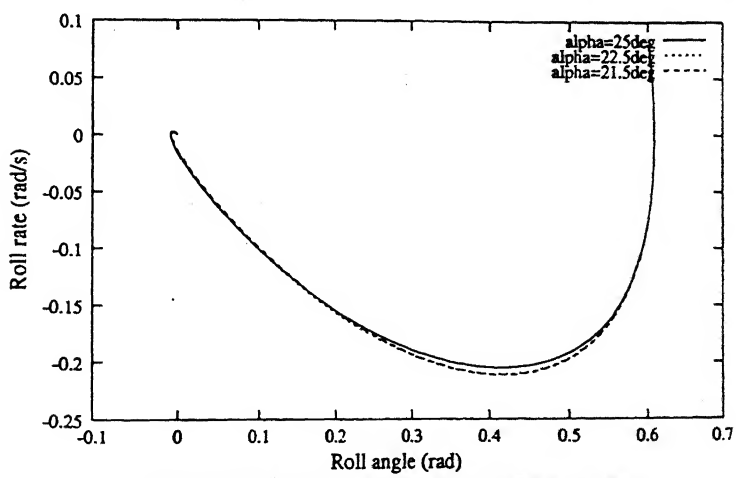

Fig.(3.8c) Phase plane plot of nonlinear feedback response
different angles of attack.

Figure 3.8: Feedback response for the third order system with initial conditions $(\phi, \dot{\phi}, \delta_A)$=(0.6 rad, 0.08 rad/s, 0 rad).

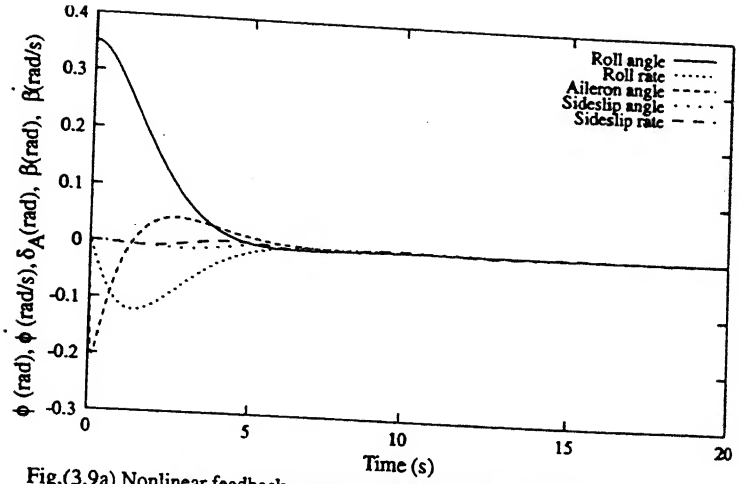

Fig.(3.9a) Nonlinear feedback response considering sideslip effects at alpha=25deg

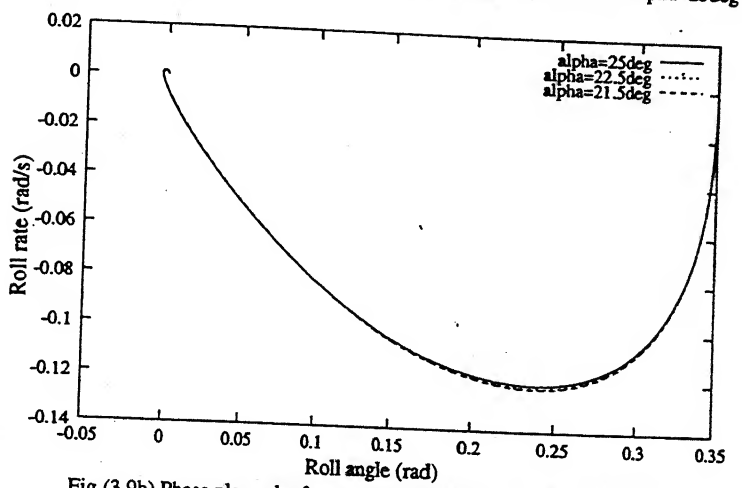

Fig.(3.9b) Phase plane plot for nonlinear feedback response considering sideslip effects at different angles of attack

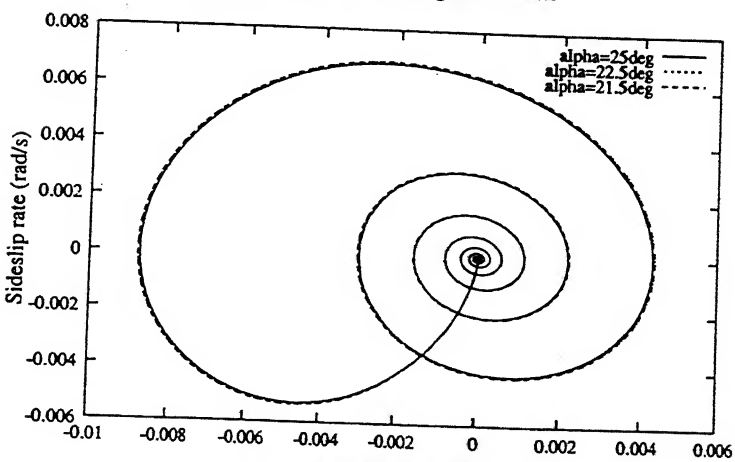

Fig.(3.9c) Phase plane plot for nonlinear feedback response considering sideslip effects at different angles of attack

Figure 3.9: Nonlinear feedback response for fifth order state variable with initial conditions $(\phi, \dot{\phi}, \delta_A, \beta, \dot{\beta})$=(0.35 rad, 0 rad/s, 0 rad, 0 rad, 0 rad/s).

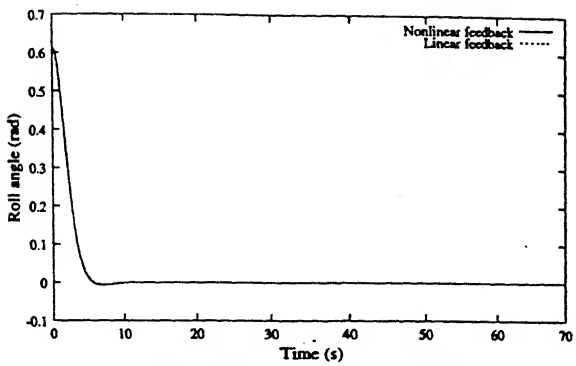

Fig.(3.10a) Variation of Roll angle with time

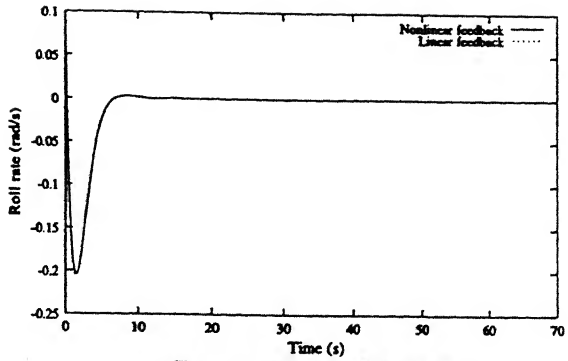

Fig.(3.10b) Variation of Roll rate with time

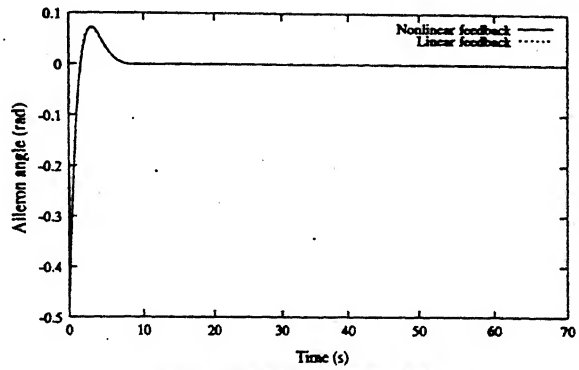

Fig.(3.10c) Variation of Aileron angle with time

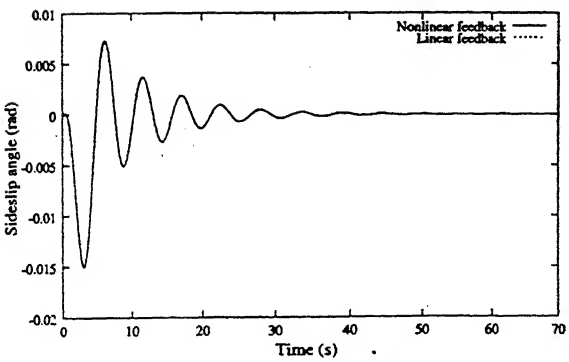

Fig.(3.10d) Variation of Sideslip angle with time

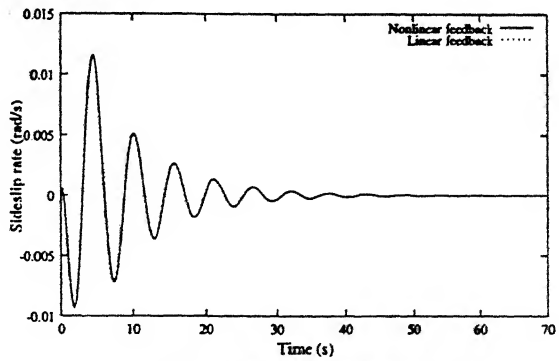

Fig.(3.10e) Variation of Sideslip rate with time

Figure 3.10: Nonlinear and linear feedback response for fifth order state variable at $\alpha = 25$ deg with initial conditions $(\phi, \dot{\phi}, \delta_A, \beta, \dot{\beta})$ =(0.6 rad, 0.08 rad/s, 0 rad, 0 rad, 0 rad/s).

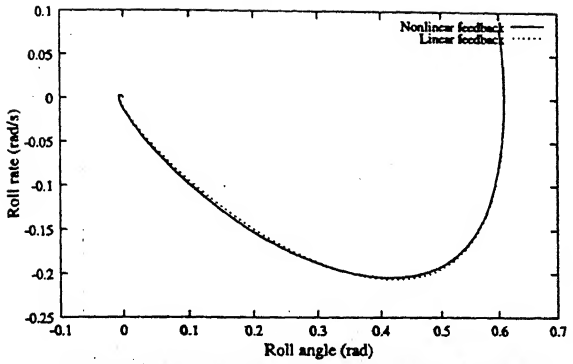

Fig.(3.11a) Phase plane plot for nonlinear and linear feedback response considering sideslip effect at alpha=25deg

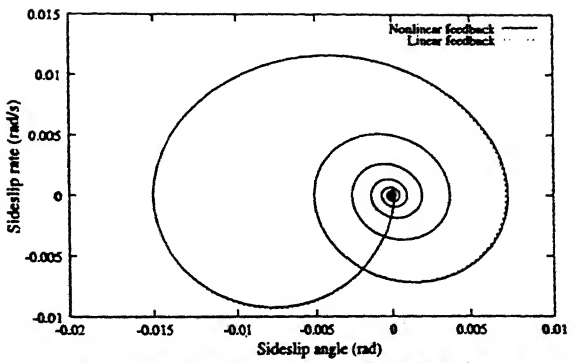

Fig.(3.11b) Phase plane plot for nonlinear and linear feedback response considering sideslip effect at alpha=25deg

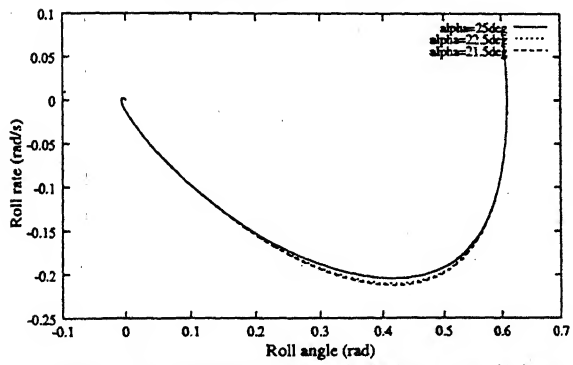

Fig.(3.11c) Phase plane plot for nonlinear feedback response considering sideslip effect at different angles of attack

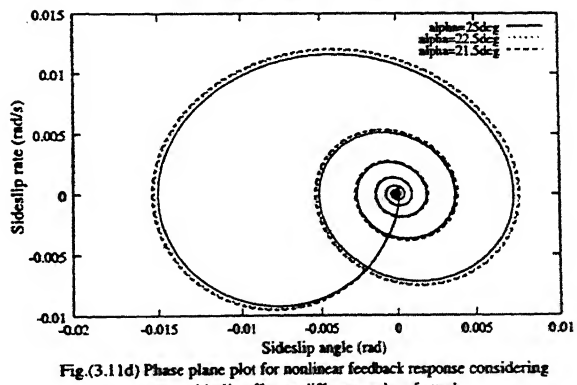

Fig.(3.11d) Phase plane plot for nonlinear feedback response considering sideslip effect at different angles of attack

Figure 3.11: Phase plane plots of closed loop system for fifth order state variable with initial conditions $(\phi, \dot{\phi}, \delta_A, \beta, \dot{\beta})$=(0.6 rad, 0.08 rad/s, 0 rad, 0 rad, 0 rad/s).

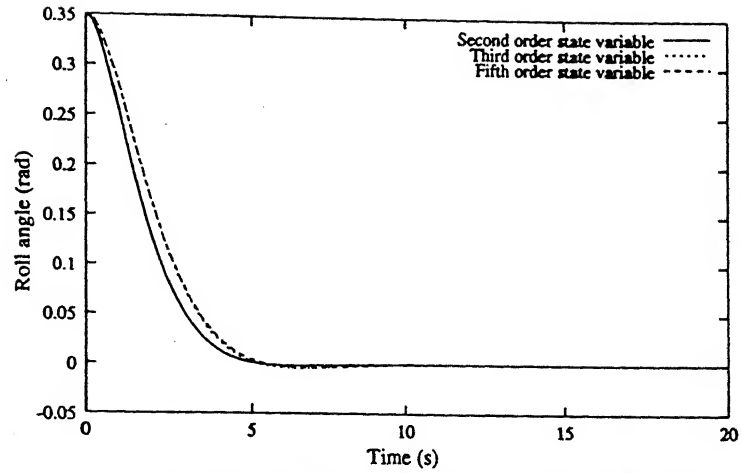

Fig.(3.12a) Nonlinear feedback response for Roll angle at alpha=25deg

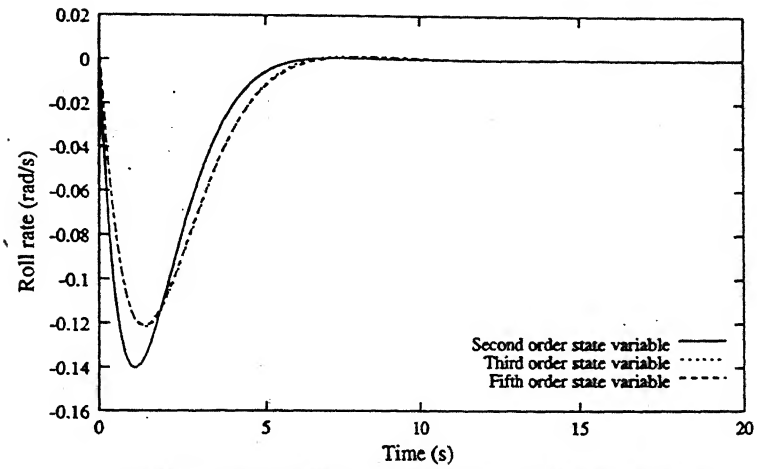

Fig.(3.12b) Nonlinear feedback response for Roll rate at alpha=25deg

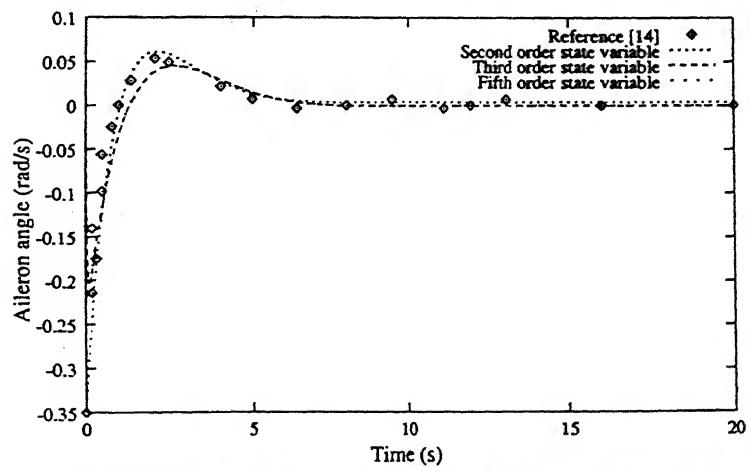

Fig.(3.12c) Nonlinear feedback response for Aileron angle at alpha=25deg

Figure 3.12: Comparison of three variables at $\alpha = 25$ deg as their order of state changes.

Chapter 4

CONCLUSIONS

A scheme has been applied for controlling the wing rock motion of aircraft flying at angles of attack near stalling onset, where optimal solution of nonlinear system is obtained by using Lyapunov function and performance index, which are both positive definite. Earlier, this method had been used for obtaining the solution of second order state variable system, but in this thesis, it has been extended to third and fifth order state variable system. Both open loop and closed loop systems have been considered. The plots obtained for open loop system have demonstrated limit cycle motion of the model when it is not in equilibrium position. The phase plane plots have shown that the limit cycle amplitude depends on angle of attack and not on initial conditions. It has been observed that sideslip angle can also initiate wing rock motion if dihedral effect considered is quite small. For the closed loop system, both nonlinear and linear feedback responses have been obtained. From these plots, we can observe that both nonlinear and linear feedback controls are equally effective for supressing the wing rock motion of our model. According to the expectation, the actuator considered in third and fifth order state variable system increases the stabilization time of the model. As observed for the fifth order state variable system, roll angle, roll rate and aileron angle stabilize in very less time, but the disturbance in sideslip angle and sideslip rate, although small in magnitude, stays for quite long time. It is to be noted that

in Ref. [12], it has been assumed that $\phi = 2\beta$, but from the plots obtained for our model, no such relation has been observed. This difference can either be due to wrong assumption or due to different model considered in Ref. [12]. Whatever ever be the reason, but it is certain that such assumption cannot be considered blindly.

In this work, variations in flight conditions have not been considered. So, considering the practical aspect of the work, if there is a provision made which can update the coefficients of the aircraft as the flight condition changes, then these optimal control equations can be utilised for controlling the wing rock motion of the actual aircraft. Future scope of the work is that, the nonlinearities in the actuator can also be considered which have been neglected in this thesis. It has been assumed that the wings remain straight during the flight, which may not be so especially when the aircraft is undergoing wing rock motion. So, the structural stiffness of the wings may also be taken into account, which has been neglected in this work.

Bibliography

[1] Nguyen, L. T., Yip, L., and Chambers, X., Jr., "Self-Induced Wing Rock of Slender Delta Wings," *AIAA Paper*, 81-1883, Aug. 1981.

[2] Levin, D. and Katz, J., "Dynamic Load Measurements with Delta Wings Undergoing Self-Induced Roll-Oscillations," *Journal of Aircraft*, Vol. 21, Jan. 1984, pp. 30-36.

[3] Ericsson, L. E., "The Fluid Mechanics of Slender Wing Rock," *Journal of Aircraft*, Vol. 21, May 1984, pp. 322-328.

[4] Ericsson, L. E., Mendenhall, M. R., and Perkins, S. C., Jr., " Review of Forebody-Induced Wing Rock," *Journal of Aircraft*, Vol. 33, March-April 1996, pp. 253-259.

[5] Ross, A. J., "Investigation of Nonlinear Motion Experienced on a Slender-Wing Research Aircraft," *Journal of Aircraft*, Vol. 9, Sept. 1972, pp. 625-631.

[6] Schmidt, L. V., "Wing Rock Due to Aerodynamic Hysteresis," *Journal of Aircraft*, Vol. 16, March 1979, pp. 129-133.

[7] Konstadinopoulos, P., Mook, D. T., and Nayfeh, A. H., "Subsonic wing Rock of Slender Delta Wings," *Journal of Aircraft*, Vol. 22, March 1985, pp. 223-228.

[8] Nayfeh, A. H., Elzebda, J. M., and Mook, D. T., "Analytical Study of the Subsonic Wing Rock Phenomenon for Slender Delta Wings," *Journal of Aircraft*, Vol. 26, Sept. 1989, pp. 805-809.

[9] Hsu, C. H., and Lan, C. E., "Theory of Wing Rock," *Journal of Aircraft*, Vol. 22, Oct. 1985, pp. 920-924.

[10] Luo, J., and Lan, C. E., "Control of Wing Rock Motion of Slender Delta Wings," *Journal of Guidance, Control and Dynamics*, Vol. 16, No. 2, 1993, pp. 225-231.

[11] Monahemi, M. M., and Krstic, M., "Control of Wing Rock Motion Using Adaptive Feedback Linearization," *Journal of Guidance, Control and Dynamics*, Vol. 19, No. 4, 1996, pp. 905-912.

[12] Singh, S. N., Yim, W., and Wells, W. R., "Direct Adaptive and Neural Control of Wing Rock Motion of Slender Delta Wings," *Journal of Guidance, Control and Dynamics*, Vol. 18, No. 1, 1995, pp. 25-30.

[13] Araujo, A. D., and Singh, S. N., "Variable Structure Adaptive Control of Wing Rock Motion of Slender Delta Wings," *Journal of Guidance, Control and Dynamics*, Vol. 21, No. 2, 1998, pp. 251-256.

[14] Shue, S. P., Sawan, M. E., and Rokhsaz, K., "Optimal Feedback Control of a Nonlinear System: Wing Rock Example," *Journal of Guidance, Control and Dynamics*, Vol. 19, No. 1, 1996, pp. 166-171.